Remote Sensing of Environment 168 (2015) 301–315

Contents lists available at ScienceDirect

Remote Sensing of Environment

journal homepage: www.elsevier.com/locate/rse

Distribution of near-surface permafrost in Alaska: Estimates of present and future conditions

Neal J. Pastick [a,g,*], M. Torre Jorgenson [b], Bruce K. Wylie [c], Shawn J. Nield [d], Kristofer D. Johnson [e], Andrew O. Finley [f]

[a] Stinger Ghaffarian Technologies, Inc., Sioux Falls, SD 57198, USA
[b] Alaska Ecoscience, Fairbanks, AK 99709, USA
[c] U.S. Geological Survey Earth Resources Observation and Science Center, Sioux Falls, SD 57198, USA
[d] Natural Resource Conservation Service, U.S. Department of Agriculture, Palmer, AK 99645, USA
[e] Northern Research Station, U.S. Department of Agriculture Forest Service, Newtown Square, PA 19073, USA
[f] Department of Forestry and Geography, Michigan State University, East Lansing, MI 48824, USA
[g] Department of Forest Resources, University of Minnesota, St. Paul, MN 55108, USA

ARTICLE INFO

Article history:
Received 30 January 2015
Received in revised form 14 July 2015
Accepted 16 July 2015
Available online 31 July 2015

Keywords:
Alaska
Data mining
Pedometrics
Near-surface permafrost
Machine learning
Remote sensing

ABSTRACT

High-latitude regions are experiencing rapid and extensive changes in ecosystem composition and function as the result of increases in average air temperature. Increasing air temperatures have led to widespread thawing and degradation of permafrost, which in turn has affected ecosystems, socioeconomics, and the carbon cycle of high latitudes. Here we overcome complex interactions among surface and subsurface conditions to map near-surface permafrost through decision and regression tree approaches that statistically and spatially extend field observations using remotely sensed imagery, climatic data, and thematic maps of a wide range of surface and subsurface biophysical characteristics. The data fusion approach generated medium-resolution (30-m pixels) maps of near-surface (within 1 m) permafrost, active-layer thickness, and associated uncertainty estimates throughout mainland Alaska. Our calibrated models (overall test accuracy of ~85%) were used to quantify changes in permafrost distribution under varying future climate scenarios assuming no other changes in biophysical factors. Models indicate that near-surface permafrost underlies 38% of mainland Alaska and that near-surface permafrost will disappear on 16 to 24% of the landscape by the end of the 21st Century. Simulations suggest that near-surface permafrost degradation is more probable in central regions of Alaska than more northerly regions. Taken together, these results have obvious implications for potential remobilization of frozen soil carbon pools under warmer temperatures. Additionally, warmer and drier conditions may increase fire activity and severity, which may exacerbate rates of permafrost thaw and carbon remobilization relative to climate alone. The mapping of permafrost distribution across Alaska is important for land-use planning, environmental assessments, and a wide-array of geophysical studies.

1. Introduction

Climate change has led to an increase in high-latitude air temperatures that are nearly double that of the global average (Intergovernmental Panel on Climate Change (IPCC), 2007). This increase in air temperature has led to widespread thawing and degradation of permafrost (Jorgenson, Racine, Walters, & Osterkamp, 2001; Jorgenson, Shur, & Pullman, 2006), which has associated impacts on ecosystems, socioeconomics, and the carbon cycle of high latitudes. Climate warming is projected to continue in the Northern Hemisphere through the 21st Century (IPCC, 2013), where permafrost is currently estimated to underlay approximately 22% of the land surface (Brown, Ferrians, Heginbottom, & Melnikov, 1997). Further warming could cause ground temperature increases, a thickening of the active layer, talik formation, changes in hydrology and topography, remobilization of carbon pools, coastal erosion, and damages to infrastructure (Chapin et al., 2000; Grosse et al., 2011; Jorgenson et al., 2010, 2013; Larsen et al., 2008; Osterkamp et al., 2009; Walvoord & Striegl, 2007). Despite permafrost's influence on ecosystem structure and functions, relatively little has been done to quantify permafrost properties across large areas and in great detail. While generalized and small-scale maps of permafrost properties exist (e.g. Brown et al., 1997; Jorgenson, Yoshikawa, et al., 2008), these map products do not account for important and local factors that influence permafrost systems. The development of spatially detailed information

* Corresponding author at: Stinger Ghaffarian Technologies, Inc., Sioux Falls, SD 57198, USA.
E-mail address: njpastick@usgs.gov (N.J. Pastick).

http://dx.doi.org/10.1016/j.rse.2015.07.019
0034-4257/

of permafrost properties is important because it can serve as an input into models predicting permafrost change. Thus, additional data and integrative approaches are needed to adequately observe and monitor permafrost (National Research Council, 2014).

Detection and monitoring of permafrost is difficult, however, because it is a subsurface condition of the ground, heterogeneous in nature, and largely found in remote locations (Riseborough, Shiklomanov, Etzelmüller, Gruber, & Marchenko, 2008). Spatial modeling of permafrost properties have largely been conducted at coarse-scale resolutions (>2 km × 2 km) (e.g. Brown et al., 1997; Jafarov, Marchenko, & Romanovsky, 2012; Lawrence & Slater, 2005; Marchenko, Romanovsky, & Tipenko, 2008), which do not represent fine-scale differences in permafrost conditions and are unsuitable for land-use planning and environmental assessments (Zhang, Olthof, Fraser, & Wolfe, 2014). Furthermore, accuracy assessments conducted at coarse scales can be unreliable because of differences in scale between maps and field observations, and assessments tend to lack a diverse set of field observations for thorough validation and calibration. More recently, several studies have applied process-based or transient models to improve representation of permafrost properties and dynamics at high resolutions (Panda, Marchenko, & Romanovsky, 2014a,b; Zhang, 2013; Zhang et al., 2012, 2014) for relatively small areas (i.e. <25, 000 km^2) in Alaska and Canada. However, because of high computational needs and the lack of detailed soils data needed for process-based or transient simulations, these approaches are currently impractical for mapping permafrost across extremely large areas. Statistical-empirical models have also been successfully applied to larger areas by quantifying relations between permafrost properties and ecological factors influencing the distribution of permafrost (Bonnaventure, Lewkowicz, Kremer, & Sawada, 2012; Mishra & Riley, 2014; Pastick, Jorgenson, et al., 2014). These automated approaches have been replacing the traditional photo-interpreted, terrain-unit approach based on landform-soil associations (Jorgenson, Yoshikawa, et al., 2008; Jorgenson et al., 2014; Kreig & Reger, 1982). Statistical-empirical models are particularly robust when a diverse set of high-quality field and geospatial data are available, as demonstrated in this study.

We overcome complexities inherent in permafrost mapping through decision and regression tree modeling approaches that statistically and spatially extend field observations using remotely sensed imagery, climatic data, and thematic maps of a wide range of surface and subsurface biophysical characteristics. This novel study expands upon decades of permafrost-related research by producing the first medium-resolution (30 m × 30 m) maps of near-surface (within 1 m) permafrost (NSP), active-layer thickness (ALT: depth to surface of permafrost), and associated uncertainty estimates, throughout all of mainland Alaska. Calibrated models were then used to quantify changes in permafrost extents under varying climate scenarios while holding other biophysical factors constant. Recently created soil carbon maps and simulated changes in near-surface permafrost extent were then used to quantify frozen C pools that are potentially liable to remobilization upon thaw. Ecological factors influencing the distribution of NSP are also examined and discussed. The work presented here provides a detailed depiction of the distribution of permafrost properties in Alaska (excluding the Aleutian and Bering Sea Islands), which is important for land-use planning, environmental assessments, and a wide-array of geophysical studies.

2. Methods

2.1. Study area and field observations

Alaska (~1,500,000 km^2) is composed of a diverse set of ecosystems, and 80% of the land surface is estimated to be within permafrost zones (Jorgenson, Yoshikawa, et al., 2008). Within this study, approximately 17,000 field measurements were used to represent permafrost properties across Alaska. These field observations were obtained from various soil databases and researchers, with the majority of the dataset coming from the Natural Resource Conservation Service (Clark & Duffy, 2003), ABR, Inc. (Jorgenson et al., 1999; Jorgenson, Racine, et al., 2001; Jorgenson, Roth, et al., 2001; Jorgenson, Yoshikawa, et al., 2008), and the U.S. Geological Survey and U.S. Fish and Wildlife Service (Pastick et al., 2013; Pastick, Jorgenson, et al., 2014). Field measurements of ALT and the presence–absence of NSP were collected from 1990 to 2013. To circumvent the use of seasonal frost observations, only thaw-depth measurements taken during late-season months (late July to mid-September) or measurements designated to have no NSP were used for model calibration and validation. Annual and slight seasonal variations in active layer thickness and corresponding field measurements could introduce bias within our model estimates. While temporal variability among field observations may be of some concern for ALT estimations, it is less likely to be of concern for estimations of the presence–absence of NSP because the presence–absence of permafrost is designated at a fixed depth interval and a smaller portion of the field observations would be affected by temporal variations in thaw depths. Areas classified as open water, cultivated, perennial ice/snow, bare soil, or developed areas, by the National Land Cover Database (Homer et al., 2007), were masked out in this study, as these areas are typically devoid or underlain by NSP. For instance, limited NSP field observations coinciding with areas mapped as water (n = 243), perennial ice/snow (n = 8), bare soil (n = 235), developed (n = 51), and cultivated areas (n = 33) held mean NSP probabilities/frequencies of 28%, 88%, 21%, 25%, and 9%, respectively.

Though the field observations were unevenly distributed across Alaska (Fig. 1), the samples represent all major ecoregions (Nowacki, Spencer, Brock, Fleming, & Jorgenson, 2001), land cover types, and surficial deposits and soil textures (Jorgenson, Yoshikawa, et al., 2008). Field observations of the presence–absence of NSP (n = 16,786; Present = 4322; Absent = 12,464) followed temperature gradients as expected, with more observations of the presence of NSP in colder regions and more observations of the absence of NSP in warmer regions of Alaska. The mean, median, standard deviation, and coefficient of determination, of those NSP measurements where the ALT was fully resolved (Fig. 2; n = 4834), were 58 cm, 49 cm, 32 cm, and 54%, respectively. Field observations were also used to assess environmental factors influencing the distribution of NSP, as discussed below.

2.2. Environmental predictors

Geospatial datasets served as environmental predictors in our permafrost models and as a continuous estimation surface to which we could apply predictive models. For the purposes of this study, environmental predictors were resampled to a 30-m spatial resolution to better match the scale of our field observations and the spectral information used in this study. Environmental predictor information was then extracted to each point observation, compiled into a modeling database, and incorporated into variable selection analyses. We explored the utility of a large number of geospatial datasets, which can help depict various surface and subsurface conditions, because permafrost responds to a wide range of ecological factors and is covered by surface vegetation and soil within the active layer.

2.2.1. Topography

Regional topographic effects can influence permafrost properties where permafrost conditions may vary with changes in elevation, slope, and aspect (Peddle & Franklin, 1993). A downscaled 30-m resolution digital elevation model (Gesch et al., 2002) and derived terrain attributes (i.e. slope, aspect, potential incident radiation, and a compound topographic index) were incorporated into our analyses, as these attributes can serve as proxies for soil moisture and run-off, and incident radiation. The compound topographic index is a steady-state wetness index (Gessler, Moore, McKenzie, & Ryan, 1995) and a function of both slope and flow direction. Potential incident radiation was calculated

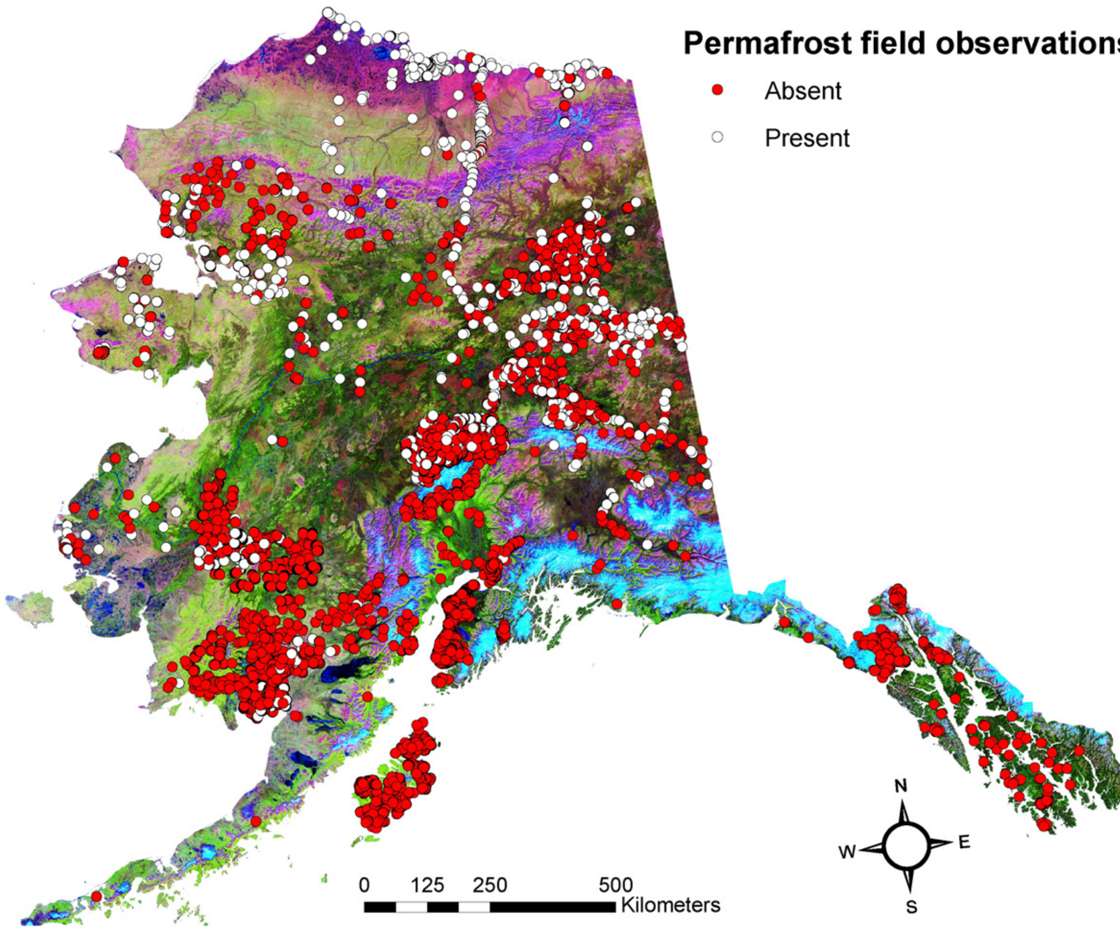

Fig. 1. Alaska overlain with presence–absence of near-surface (within 1 m) permafrost sample sites and a Landsat 7 Enhanced Thematic Plus mosaic (false color composite [red, green, blue: 5, 4, and 3]).

using those methods described by McCune and Keon (2002) and is a function of aspect and latitude/longitude. Micro-topography can also influence local-variations in permafrost distribution and associated terrain attributes (Lara et al., 2015; Wainwright et al., 2015), but fine-scale topographical datasets are currently unavailable for all of Alaska.

2.2.2. Vegetation and land surface characteristics

Vegetation characteristics have strong physically-based linkages with permafrost properties that involve vegetation canopy's influence on surface energy balances, relations between soil moisture and vegetation that affects thermal properties, and vegetation response to disturbances with varying successional trajectories having different organic matter thickness important for heat transfer (Hall, 1982; Jiang et al., 2015; Nauta et al., 2015; Smith & Burgess, 2004; Zhang, Chen, & Cihlar, 2003). Subsequently, our analyses made use of 2001 national land cover database and wetland (Whitcomb, Moghaddam, McDonald, Kellndorfer, & Podest, 2009) data to differentiate vegetation types that can be indicative of permafrost presence/absence. Previous remote

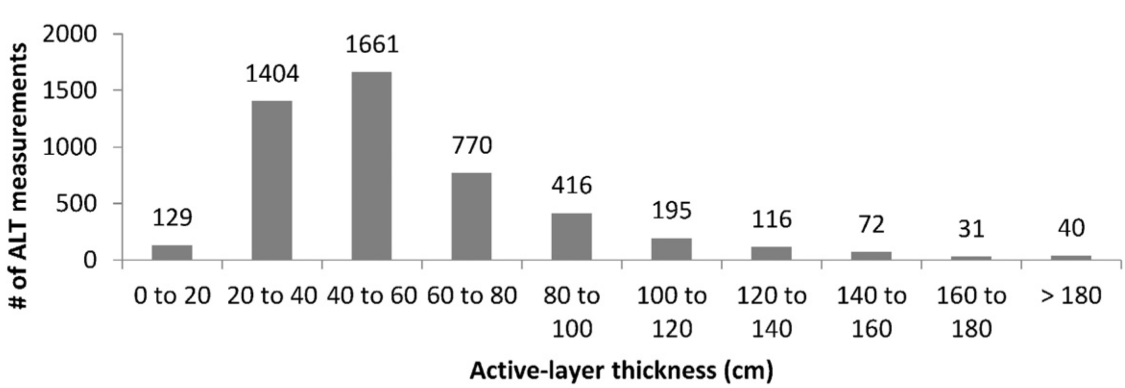

Fig. 2. The number of fully resolved active-layer thickness (ALT) measurements in 20 cm depth intervals.

sensing-based studies have also made use of spectral information to quantify land surface features associated with permafrost processes, and permafrost properties indirectly (Belshe, Schuur, & Grosse, 2013; Duguay, Zhang, Leverington, & Romanovsky, 2005; Hall, 1982; Kääb, 2008; Leverington & Duguay, 1997; Lewkowicz & Duguay, 1999; McMichael, Hope, Stow, & Fleming, 1997; Morrissey, Strong, & Card, 1986; Nguyen, Burn, King, & Smith, 2009; Peddle, Foody, Zhang, Franklin, & Ledrew, 1994; Peddle & Franklin, 1993). Spectral information and vegetation indices, as derived from a late-season Landsat 7 Enhanced Thematic Mapper Plus mosaic (2008–2011), were introduced into our analyses because of their ability to depict and accentuate biophysical properties and surface conditions (Laidler & Treitz, 2003; Stow, Hope, McGuire, et al., 2004) that are not evident in generalized vegetation maps. Specifically, the normalized difference infrared index (NDII) and normalized difference water index (NDWI) were introduced because of known sensitivities to burn severity, plant canopy characteristics (e.g. biomass, leaf area index) and soil moisture content, all of which are important factors influencing permafrost properties. The normalized difference vegetation index (NDVI) and green normalized vegetation index (GNDVI) were introduced because of sensitivity to plant productivity and greenness, which can serve as surrogates for permafrost presence/absence (Belshe et al., 2013). The near-infrared (~0.77–0.90 μm) and mid-infrared (~2.09–2.35 μm) bands of Landsat imagery have been used to quantify vegetation recovery after disturbance (Hall, Ormsby, Johnson, & Brown, 1980; Veraverbeke et al., 2012) and organic matter consumption in boreal forest fires in Alaska (Barrett, McGuire, Hoy, & Kasischke, 2011; Rogers et al., 2014), both of which share strong linkages to permafrost response to fire. While temporal differences between spectral datasets and land cover classifications exist, we assume these differences have little effect on model estimations because a limited number (n ~ 500) of observations represent areas that have undergone major change (i.e. burns) between 2001 and 2010. Readers are referred to Table A1 for an exhaustive list of spectral and vegetation data introduced into our analyses.

2.2.3. Climate

As permafrost distributions are strongly influenced by past and present climate, climatic indices were also included within our analyses and obtained from the Scenarios Network for Alaska and Arctic Planning website (https://www.snap.uaf.edu/). Historical and projected climate data were downscaled (777-km to 30-m spatial resolution), and consisted of decadal averages (i.e. 1990 to 2010) of seasonal and annual mean indices. While climatic data are relatively coarse, as compared to other datasets used within model development, climate data were mainly used to describe regional differences in permafrost distribution. Average annual and seasonal precipitation information consisted of summer (i.e. June, July, and August) and winter (i.e. December, January, and February) estimates. Decadal averages of day of freeze and thaw, length of growing seasons, and annual mean air temperatures were also included within our permafrost analyses. See Section 2.4 for details on climate data used for future permafrost predictions.

2.3. Predictive Modeling and Mapping

Decision and regression trees are a non-parametric set of knowledge-driven machine-learning algorithms that provide an automated means of recognizing patterns to solve non-linear problems in high-dimensional input space (Hastie, Tibshirani, & Friedman, 2009). Decision and regression tree ensembles were developed, using commercially available See5 and Cubist software (Quinlan, 2003), to estimate presence–absence of NSP and ALT, respectively. Field observations and co-located environmental predictor information represent examples that were used for attribute selection, model calibration, and model testing as described below.

While it is important to exhaustively account for environmental factors influencing permafrost distributions, it is also imperative to be selective because errors within various geospatial datasets can be propagated through our modeling and mapping approach. Here we selected environmental predictors using various data mining techniques (i.e. correlation-based feature evaluations and winnowing) and expert judgment. Winnowing (Quinlan, 2003) and correlation-based feature evaluations (Hall, 2000) were used to evaluate the worth of environmental predictors by searching through the feature space, using a forward-selection greedy algorithm (using minimum error as the criteria), and discarding those predictors that are found to be adverse to the predictive capacity of the model or those that have significant correlations with other predictors. Within this study, 28 environmental predictors were incorporated into attribute selection analyses. After useful environmental predictors were identified, a predictor usage metric was calculated to assess the individual importance of each of the environmental predictors employed within NSP model development. This usage metric is defined as the number of training examples for which the value of the environmental predictor is used in predicting the presence–absence of NSP, divided by the total number of cases in the model development database. Note that these metrics only identify predictor variables that were most frequently used in model development and do not necessarily reflect all factors influencing the distribution of permafrost. For instance, shallow lithology also influences soil-thermal conductivities but was only implicitly accounted for in these analyses through the use of spectral and topographical datasets.

Selected attributes were then incorporated into a binary decision tree model to estimate the presence–absence and probability of NSP, with 30 observations required to make a classification (i.e. thirty observation per terminal leaf). Piecewise linear regression tree models were then developed to estimate ALT in areas where NSP was estimated to be present, and by using ALT measurements coinciding with these areas and those within the 1-m depth interval. We sought to construct parsimonious models, where training and test accuracies are similar, to insure that the model generalizes well to new locations. Here models were constructed using a top-down greedy algorithm that partitions the feature/hypothesis space using a gain ratio (i.e. minimum error) as splitting criteria (Quinlan, 1993). In the case of the ALT regression tree model, Cubist makes decision splits that minimize the prediction squared error. Decision tree classifiers also provide a probability or confidence estimate using the actual distribution of presence–absence observations in each leaf of the tree, rather than assigning the leaf entirely to the majority class (i.e. presence or absence of NSP). Because we used an ensemble/boosting technique (Quinlan, 1996), estimates represent the mean (probability, confidence, ALT) or majority (presence–absence of NSP) values across multiple trees, which are typically more robust than estimates derived from a single model. Moreover, boosting can reduce the bias of a weak learner by forcing the model to concentrate on different parts of the input space, which were more prone to error, and can also reduce model variance and improve model stability (Freund & Schapire, 1996). Calibrated models were then applied to the environmental predictors (i.e. geospatial dataset) to produce spatial estimates of presence–absence and probability of NSP, and ALT. Environmental controls on estimated and field observation NSP were assessed by examining the structure of the decision tree, and by converting influential environmental predictor data into distinct zones and calculating averages and standard deviation of NSP in each zone. We assumed a binomial distribution (i.e. absence $= 0$; presence $= 1$) when calculating the mean (ratio between observations of NSP and the total number of observations) and standard deviation (σ) of observed NSP probabilities in each zone:

$$\sigma = \sqrt{np(1-p)} \tag{1}$$

where n is the number of measurements and p is the probability of encountering NSP.

Accuracy assessments of the models and resulting maps were conducted using 10-fold cross validations (Martin et al., 2011) and independent tests. Cross-validation assessments utilized the entire dataset by randomly dividing into training and test datasets 10 times, such that all measurements were used once as validation. For binary presence–absence NSP predictions, an average of ten 10-fold cross validations was performed to achieve a better representation of model accuracies. Independent tests were also conducted using randomly withheld field observations and field observations obtained after model calibration. Field measurements obtained after model calibration are those described in recent studies (Jelinksi, 2014; B. Minsley, Personal communication, May 20th, 2015; Romanovsky & Cable, 2014; Swanson, 2012) and observations where NSP could not be determined were removed for direct comparison with our maps. Confusion matrices were made to highlight overall, producers, and users training accuracies (see Congalton, 1991) when comparing withheld field data with that of presence–absence NSP estimations. For the continuous estimations of ALT, withheld field measurements and map predictions were used to calculate mean estimation error (MAE), mean bias errors (MBE), relative mean estimation error (rMAE), relative mean bias error (rMBE), and the coefficient of determination (Willmott & Matsuura, 2005). These error matrices were calculated to evaluate the measure of overall model performance and model bias.

2.4. Future predictions and vulnerability assessments

Future projections of climate indices were available under 3 emission scenarios of varying severity (i.e. low = B1; moderate = A1B; severe = A2), as estimated by 5 models (i.e. cgcm31, cm2, medres, echam5, hadcm3) that perform best across Alaska and the Arctic (Walsh, Chapman, Romanovsky, Christensen, & Stendel, 2008). Here we used future projections of climatic estimates, as averaged across the 5 models for each scenario, to assess possible landscape-level changes to permafrost extents in Alaska. The calibrated NSP model was forced by future climate data (i.e. 2050 and 2090) to estimate potential changes in NSP distribution during the 21st Century. We note, however, that the complex interactions and feedbacks affecting the resilience and vulnerability of permafrost to climate change (Jorgenson et al., 2010) lead to substantial uncertainty in estimating future permafrost distributions. Moreover, these estimations and analyses help demonstrate large uncertainties associated with estimating changes in permafrost extents and help reiterate the need for precise baseline estimates of permafrost distribution.

In addition to future estimates of NSP extents and probabilities, we utilize recently created soil organic layer (Wylie, Pastick, Johnson, Bliss, & Genet, in press) and ice content (Jorgenson, Yoshikawa, et al., 2008) maps to determine areas that are predisposed to thermokarst development. Lowland areas with moderate to high ground-ice contents and organic soils are vulnerable to thermokarst formation because increases in soil temperature can lead to subsidence of the land surface due to melting ground ice. Because substantial pools of frozen soil organic carbon are potentially liable to remobilization and decomposition upon permafrost thaw (Schuur et al., 2015), recently created frozen mineral and organic soil carbon maps (Wylie et al., in press) were used to assess the amount of soil carbon that may be susceptible to climate-induced permafrost degradation. Those areas predicted to undergo disappearance of NSP, under the A1B emission scenario, were identified and frozen soil carbon estimates were summed over that area.

3. Results and discussion

3.1. Model performance and map accuracy

A total of 19 environmental predictors were used during NSP model development (Table A1), while 8 predictors (denoted by "—") were winnowed or discarded prior to NSP model calibration. Decision and regression tree models were then applied to useful environmental predictors to produce maps of the probability of NSP (Fig. 3a), presence–absence of NSP (Fig. 3b), and ALT (Fig. 3c) throughout Alaska. Note, however, because there are errors within each of these predictor variables, each pixel of the output maps has its own level of confidence or error. To better represent errors, an error map was generated for the NSP product and represents confidence estimates of each classification in the decision tree (Fig. 4). As permafrost is usually found within the first meter of the soil (Fig. 2) our near-surface permafrost map represents overall permafrost distribution in Alaska, except for mountainous areas with rocky soils. Masked out areas (i.e. water, ice/snow, unvegetated areas) are not modeled, with the unvegetated areas being predominately barren and developed areas (Homer et al., 2007).

Overall training and averaged cross-validation accuracies for the calibrated NSP model were 87% and 85%, respectively. In addition to the overall cross-validation test accuracy, the cross-validation confusion matrix (Table 1) depicts distinct errors (i.e. commission or omission) or accuracies (i.e. user or producer) as they relate to each class prediction (i.e. absent or present). Model estimations of the absence of NSP held higher user and producer accuracies than those of the presence of NSP, suggesting that the calibrated NSP model is more accurate at predicting areas lacking NSP throughout the study domain. Moreover, user and producer errors are similar for each distinct class comparison, indicating little bias in either over or under estimations of each class. Because cross-validation accuracy assessments do not reflect how map accuracies vary spatially, additional independent tests were conducted using field measurements obtained after model calibration. Field measurements ($n = 245$) obtained from Jelinksi (2014) and Swanson (2012), along transects representing major landforms in the Seward Peninsula and the Brooks Mountain Range, indicated that the overall map accuracy for these areas was 86% (95% CI: 81.8, 90.5), similar to the overall cross-validation accuracy for the entire state. Interestingly, producer and user accuracies were lower for estimations of the absence of NSP (38% and 56%) than predictions of the presence of NSP (95% and 90%). However, the average field observation and mapped probability of NSP was 86% at these locations, which suggests that the probabilistic estimates are useful. Ground-temperature (1 m) measurements ($n = 21$), obtained from Romanovsky and Cable (2014) in mostly undisturbed and homogeneous areas of western Alaska, indicated that the overall map accuracy for these areas was 90% (95% CI: 77.1, 100), with an average user and producer accuracy of 94% and 83%, respectively. Errors occurring in these regions are likely due to the model's inability to predict extremely rare instances; or in this case, areas devoid of NSP in northern and western regions identified to have continuous permafrost (Jorgenson, Yoshikawa, et al., 2008). Subsequently, the converse is likely true for estimations of the presence of NSP in areas with isolated permafrost. While this may be of some concern to end users of the NSP products, it is likely of less concern to those users conducting regional- to landscape-level analyses because of the rarity of these phenomena.

Disturbance-induced change can have a large impact on permafrost dynamics and it is important to assess how well our permafrost model captures complex fire-permafrost interactions. An independent test dataset, representing measurements ($n \sim 800$) taken across burned-unburned transects in boreal landscapes in interior Alaska (B. Minsley, Personal communication, May 20th, 2015), indicate that map accuracies for these areas are reasonable with an overall accuracy of 70%. Lower accuracies in burned areas are to be expected, however, because post-fire observations were limited in this study and the heterogeneous effects of fire are difficult to quantify using remote-sensing imagery. Therefore estimates within recently disturbed areas are inherently more uncertain than other undisturbed areas. As more post-fire observations become available they can be incorporated into our data fusion approach to better quantify fire impacts on permafrost. Despite these model shortcomings, the NSP maps represent the first depiction of near-surface permafrost extents throughout Alaska derived from a large set of field observations, and will be useful for a wide-array of geophysical, hydrological, and engineering studies.

Regression tree model performance and ALT map (Fig. 3c) accuracies were also assessed with independent test datasets. For one of these

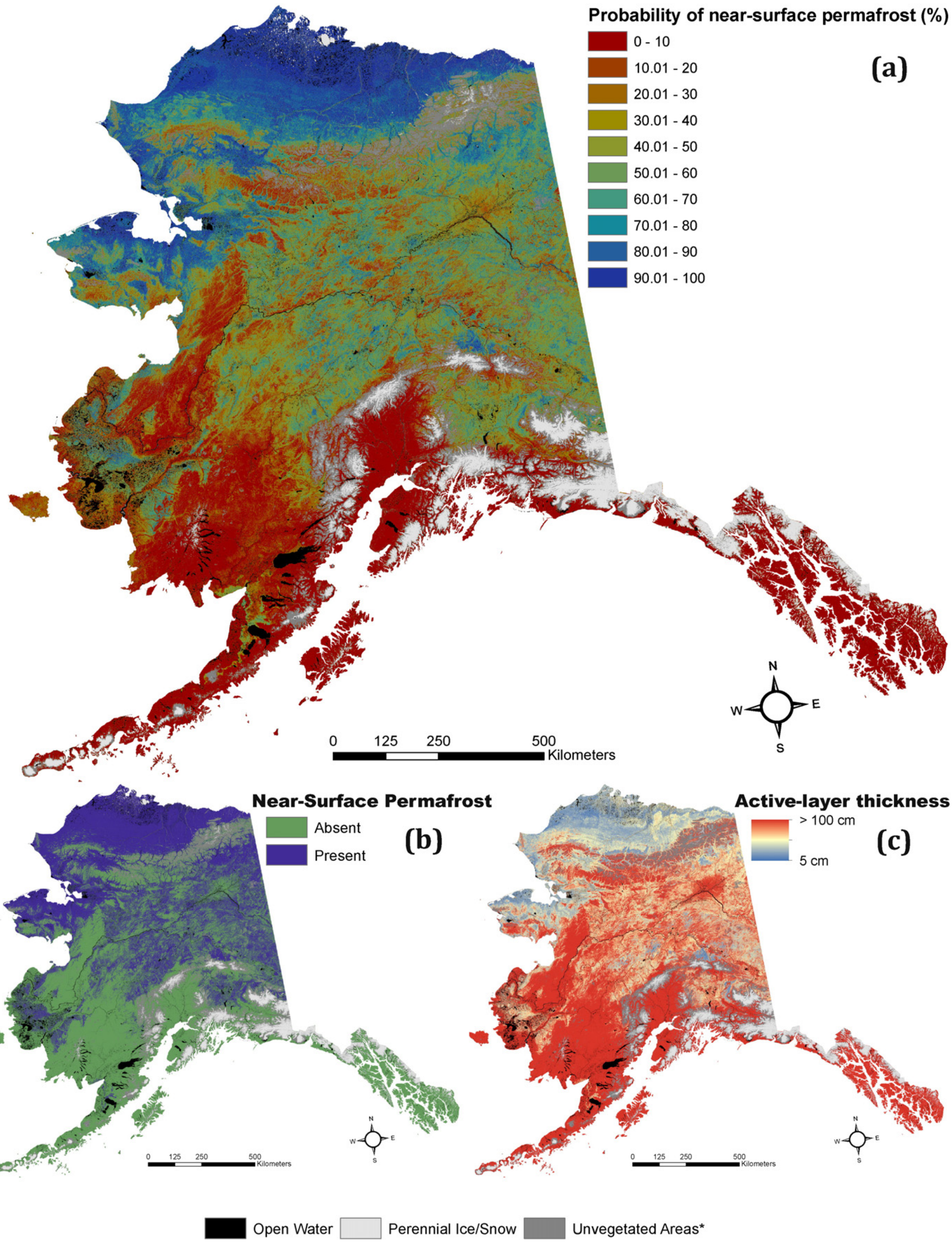

Fig. 3. Modeled maps of (a) probability of near-surface (within 1 m) permafrost (NSP), (b) presence–absence of NSP, and (c) active-layer thickness (cm) within Alaska. Map (b) was derived from map (a) using a 50% probability threshold.

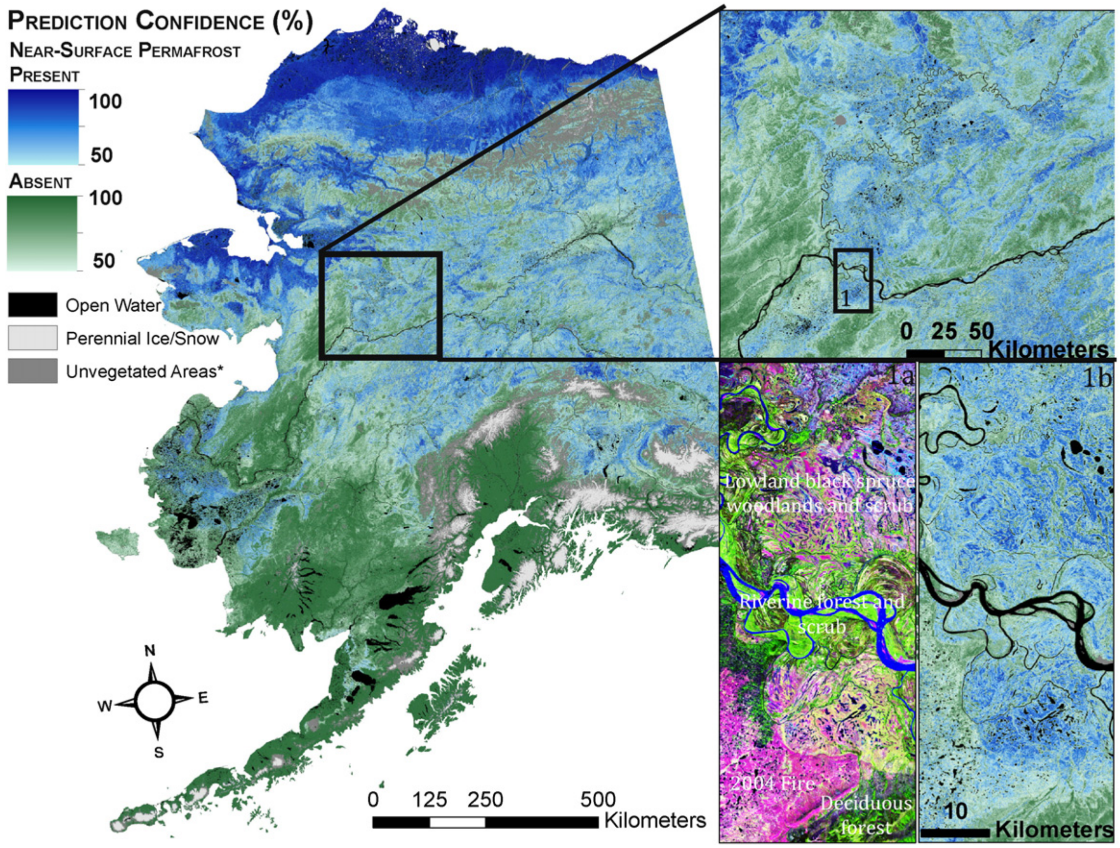

Fig. 4. Mapped confidence (%) of presence–absence of near-surface (within 1 m) permafrost (NSP) predictions with darker blues and greens indicating higher confidence. Enlarged area insets (1a) and (1b) correspond to Landsat imagery and mapped confidence of presence–absence of NSP predictions, respectively.

analyses, randomly withheld ALT field observations ($n = 216$) were compared with ALT model predictions. These observations represent a random sample of the total population of ALT measurements, within areas predicted to contain NSP, and had a mean of 47 cm, standard deviation of 21 cm, and coefficient of variation of 45%. Error matrices were calculated during these comparisons. The MAE (13 cm) and MBE (−1 cm) represent the average absolute difference and difference between withheld data and model predictions, and show that predictions were mainly underestimated. The rMAE (27%) and rMBE (0%) were moderately low and demonstrate that model predictions errors were fairly small in comparison to the actual average of withheld field observations. The correlation coefficient between predictions and withheld field data is low ($r = 0.61$) and the ALT model tended to under predict thicker ALTs (slope: 0.43). Measurements obtained after model calibration were also used as an independent test dataset and had slightly higher error values but lower relative errors (MAE = 15 cm; MBE = 8 cm; rMAE = 15%; rMBE = 1%). Similar accuracies have been achieved in previous ALT modeling efforts (Jafarov et al., 2012; Marchenko et al., 2008; Mishra & Riley, 2014; Zhang, 2013; Zhang et al., 2012, 2014), but regional studies have lacked a robust field dataset for thorough validations and have been mapped at coarse resolutions. Despite moderate ALT error rates in this study, we believe more work is needed to accurately represent the spatial variability of ALT throughout Alaska. Preliminary regression tree models, which made use of all available ALT measurements, significantly underestimated ALT greater than 1 m. This finding suggests that a purely continuous and useful estimation of ALT was not feasible using this set of field measurements, environmental predictors, and model. This is also true when ALT values were transformed (e.g. natural log) or weighted. We hypothesize that the underestimation of thicker ALT is likely due to the rarity and difficulty of observing ALT greater than a meter (Fig. 2), and because of decreased interactions or linkages between deeper permafrost and surface

Table 1
Cross-validation confusion matrix of field data compared to final predicted presence–absence of near-surface (within 1 m) permafrost class map. Producer's accuracy is defined as the number of observations designated correctly (i.e. bolded), divided by the total number of field data designated as a certain class (i.e. column total). User's accuracy is defined as the number of correctly classified observations, divided by the total number of mapped class designated as a certain class (i.e. row total). Overall accuracy is defined as total correctly classified observations divided by the total number of observations.

		Field data				
		Absent	Present	Row total	User's accuracy	95% confidence interval
Mapped	Absent	**11,234**	1248	12,482	90%	(89.5, 90.5)
	Present	1230	**3074**	4304	71%	(70.1, 72.8)
	Column total	12,464	4322	–	–	–
	Producer's accuracy	90%	71%	–	–	–
	95% confidence interval	(89.6, 90.7)	(69.8, 72.5)	–	–	–
	Overall accuracy	–	–	–	85%	(84.7, 85.8)

features represented by our set of environmental predictors. The finding of the underestimation of thick ALT coincides with results of a previous research effort (Mishra & Riley, 2014), where a geographically weighted regression model and a limited amount of field observations ($n = 142$) were used to predict ALT across Alaska.

Previous remote sensing-based studies have made use of supervised classification and statistical models (e.g. neural network, maximum likelihood, logistic regression, piecewise regression, decision trees) to map permafrost properties for smaller areas (e.g. Leverington and Duguay, 1996, Leverington & Duguay, 1997; Morrissey et al., 1986; Gangodagamage et al., 2014; Panda et al., 2010, Panda, Prakash, Jorgenson, & Solie, 2012; Pastick et al., 2013; Peddle & Franklin, 1993). For instance, Leverington and Duguay (1996) developed a neural network model for the estimation of permafrost presence–absence (accuracy > 90%) in portions of the Yukon Territory of Canada (<400 km^2) but found that the model did not generalize well to other areas, as indicated by an independent test (accuracy of 60%) in a separate study (Leverington & Duguay, 1997). Morrissey et al. (1986) used a logistic discriminant function to predict three permafrost zones at the Caribou-Poker Creeks watershed in Alaska (106 km^2), and acknowledged that the model (accuracy of 78%) was likely not portable to new locations and that accuracy tests were hampered by lack of in-situ data. Gangodagamage et al. (2014) used a piecewise linear regression model ($r^2 = 0.76$) and high-resolution topographical and Worldview-2 imagery to quantify ALT in a 5 km^2 area of Barrow, Alaska, but this study was constrained to a continuous permafrost region in Alaska. In comparison to previous studies, our study incorporated a larger number of field observations that covered a larger transition in permafrost distribution and was designed to develop parsimonious models. Furthermore, studies have shown that decision tree classifications typically outperform maximum likelihood, linear discriminant functions, and neural network classifiers in regards to classifier accuracy (Friedl & Brodley, 1997), and that decision trees are better suited to solve problems when a large number observations are available for model fitting (Perlich, Provost, & Simonoff, 2003). It is important to note, however, that our map accuracies for smaller areas may not be as good as those achieved in local mapping studies because of the inherent complexities associated with developing regional-scale mapping models.

Our decision tree approach to statistically and spatially extend a large number of permafrost observations throughout Alaska has the advantage of providing explicit probabilities and uncertainties, is computationally efficient, insensitive to noise and model overfitting, and provides insight into predictor variable usage. Current limitations of our modeling approach correspond to the depth of investigation (only explicitly consider permafrost in the first meter), parameter uncertainties (e.g. potential errors within input geospatial datasets), and temporal variability among input data. As additional field data become available, the spatial accuracy of these maps can be better assessed and models will be refined to explicitly account for deeper permafrost. Our data fusion approach would benefit from more precise and high resolution climatic, topographical and vegetation data, a tighter temporal correspondence and consistent observation depths among field data, maps of various soil properties (e.g. surficial geology, soil texture, rock fragment content, organic layer thickness) and burn severity, and the inclusion of additional remote sensing imagery (e.g. geophysical, active, passive) or derived products (e.g. soil moisture, surface deformation, land surface temperature, snow cover characteristics). Future work is needed to further develop and test data fusion approaches and algorithms for mapping soil characteristics across diverse landscapes, and to better account for disturbance factors that can affect soils.

3.1.1. Spatial variability of near-surface permafrost and active-layer thickness

Near-surface permafrost was estimated to be present on 34% of Alaska (where NSP probability ≥ 50%), with a spatial mean NSP probability and active-layer thickness of 45% and 50 cm, respectively. Masked land cover types account for approximately 22% of the landscape, with the majority being mapped as water (10%), bare soil (8%), and perennial ice/snow (4%). If field observation-based estimates of NSP are applied to these masked land cover types, then NSP is present on 38% of Alaska. Arctic and Bering Tundra ecoregions had the highest mean estimated NSP probabilities, followed by Intermontane Boreal and Coastal and Pacific Mountain Transitions (Fig. 5). Bering Taiga and Alaska Range Transitions had moderately low mean NSP probabilities, but were higher than those of the Aleutian Meadows and Coastal Rainforests.

NSP estimates were compared to a previously made permafrost map of Alaska Jorgenson, Yoshikawa, et al. (2008). Permafrost zones identified to be continuous (>90%), discontinuous (50–90%), sporadic (10–50%), isolated (>0–10%), and absent (0%) by Jorgenson, Yoshikawa, et al. (2008) were estimated to have mean NSP probabilities of 65%, 41%, 26%, 16%, and 1%, respectively. Trends between NSP field observations and permafrost zones were similar with mean NSP probabilities of 61%, 41%, 19%, 17%, and 0%. Differences between NSP probabilities and mapped permafrost extent may be indicative of localized factors not fully accounted for in zonal mapping approaches, differences in the depth of investigation (1 m versus 10 m), mapping errors within each product, difficulties in quantifying deep permafrost in rocky alpine soils, and the spatial distribution of permafrost field observations. However, users of the probabilistic map (Fig. 2a) may find that different probability thresholds can be informative. For instance, Jorgenson, Yoshikawa, et al. (2008) estimated that permafrost is absent on 20% of Alaska, which closely corresponds to the area with less than 10% NSP probability in Fig. 2a.

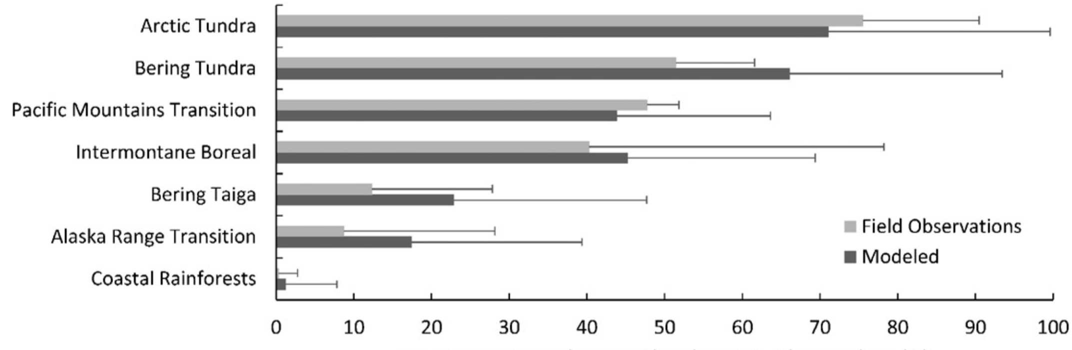

Fig. 5. Mean (±SD) probabilities of near-surface (within 1 m) permafrost by ecoregion (Nowacki et al., 2001). Ecoregions with less than 10 field observations (i.e. Aleutian Meadows and Coast Mountains Transition) are not shown here.

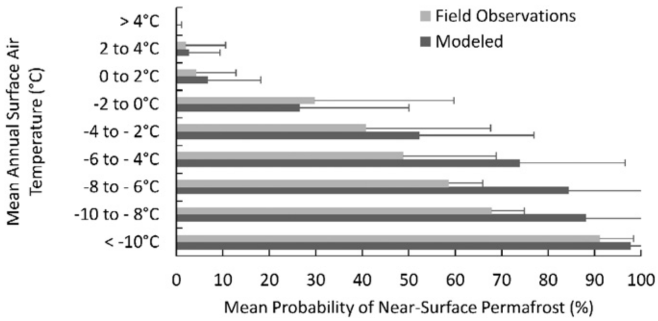

Fig. 6. Mean (±SD) probabilities of near-surface (within 1 m) permafrost by mean annual (i.e. 1990–2009) air temperature.

3.2. Environmental factors influencing the distribution of near-surface permafrost

Climatic indices, such as mean annual air temperature, date of thaw or freeze, length of growing season, and annual and winter precipitation, were the primary drivers of landscape-level NSP distributions in this study. For instance, as mean annual air temperatures (MAAT) increased from −10 °C to 0 °C, mean estimated and field-observation NSP probabilities decreased 91% and 87%, respectively, or approximately −9% per 1 °C gain (Fig. 6). Estimated and field observation NSP probabilities were greater than 90% in areas where MAATs were less than −6 °C or −9 °C, respectively. As the date of thaw increased from late-March to late-May, the mean estimated and field-observation NSP probabilities increased from 0% to 95% and 0% to 88%, respectively. This observation implies that areas with a later date of thaw are, in general, more likely to have near-surface permafrost than areas with earlier dates of thaw. As mean annual precipitation increased from 200 mm to > 1000 mm, throughout all of Alaska, mean estimated and field-observation NSP probabilities decreased from 81% to 0% and 46% to 0%, respectively. As winter precipitation (mostly in the form of snow) increased from 40 mm to 120 mm, throughout all of Alaska, mean estimated and field-observation NSP probabilities decreased from 79% to 3% and 43% to 2%, respectively. Trends between field-observation NSP probabilities and precipitation were non-linear, and associated differences between observed and estimated NSP probabilities suggest that precipitation influences permafrost on a localized scale (e.g. Intermontane Boreal).

Climate–permafrost relationships in our study were in general agreement with previous local- and landscape-scale studies (Anisimov & Nelson, 1997; Hinkel & Nelson, 2003; Hoelzle, Mittaz, Eztelmuller, & Haeberli, 2001; Jafarov et al., 2012; Johansson et al., 2013; Johnson et al., 2013; Nelson et al., 1997). MAATs ranging from −6 °C to −8 °C have been used to delineate the southern boundary of continuous permafrost (Brown & Pewe, 1973; Jorgenson, Yoshikawa, et al., 2008), similar to the −6 °C and −9 °C range we found. Snow cover, which can act as a strong insulator to permafrost or can inhibit thermal fluxes between the atmosphere and the ground (Osterkamp & Romanovsky, 1996; Stieglitz, Déry, Romanovsky, & Osterkamp, 2003), also was found to be a strong driver of our modeled permafrost distribution. These strong climatic drivers indicate that projected increases in temperature and precipitation during the 21st Century (Walsh et al., 2008) will cause widespread permafrost degradation with large ecological consequences. Large pools of previously frozen soil carbon may become remobilized (Schaefer, Lantuit, Romanovsky, Schuur, & Witt, 2014; Schuur et al., 2008). Warmer and wetter climates also may lead to increases in vegetation productivity, and longer growing seasons (Keyser, Kimball, Nemani, et al., 2000; Myneni, Keeling, Tucker, et al., 1997), all of which are inversely related to NSP extents. Note that while present and historical climates are the dominant factor influencing the distribution of permafrost, climate-ecosystem-permafrost interactions differ between permafrost zones (Shur & Jorgenson, 2007).

Spectral information was also an influential predictor during NSP model development (Table A1). In this study, the near-infrared band of the Landsat Enhanced Thematic Plus dataset (band 4) was used as often as certain climatic indices, indicating that certain surface features (e.g. vegetation or soil moisture) are good indicators of the presence or absence of NSP across the landscape. Note that this is the only inverse relation between NSP probability and spectral data (increase in reflectance results in a decrease in NSP probability), except for vegetation indices, and trends between field observations and near-infrared spectral values were similar. Furthermore, extremely high near-infrared reflectance values tended to correspond to areas with relatively little above ground biomass (e.g. bare soil, lichens) and uplands in the Nulato Hills and southern Alaska. As late-season NDII values (with a range of −1 to 1) increased from 0 to 0.5, mean estimated and field-observation NSP probabilities decreased from 73 to 1% and 66% to 0%, respectively. NDVI (and gNDVI) and NSP probabilities were also inversely related, where higher NDVI values (e.g. productive vegetation) generally correspond to areas less likely to be underlain by NSP.

Spectral–permafrost relationships in our study reaffirm the importance of various biophysical conditions to permafrost found in other studies (Belshe et al., 2013; Gangodagamage et al., 2014; McMichael et al., 1997; Morrissey et al., 1986; Nguyen et al., 2009; Panda et al., 2012; Pastick, Jorgenson, et al., 2014). Because the normalized difference infrared index (NDII) values are indicative of moisture conditions of vegetation and soil (Ji et al., 2012), the negative relationship between NDII and permafrost probabilities indicates that moist vegetation and dry soils are generally less likely to be underlain by NSP than drier vegetation or wetter soils in Alaska. Correspondingly, Raynolds and Walker (2008) identified similar inverse relations between permafrost extents and a related normalized difference vegetation index. If plant productivity trends in Alaska persist (Beck & Goetz, 2011), increases in land surface albedo, evapotranspiration, and above ground biomass are likely to occur (Pearson et al., 2013), which can serve as a positive or negative feedback to the permafrost system.

Mean estimated and field-observation NSP probabilities varied approximately fifteen- and four-fold across land cover types in Alaska, respectively. Overall mean estimated and field-observation NSP probabilities were lower for deciduous forest (6 and 13%), grassland/herbaceous (9 and 3%), and mixed forest (11 and 10%) than those observed for evergreen forest (27 and 26%), shrub/scrub (34 and 23%), wetlands (44 and 30%), dwarf scrub (65 and 35%), and sedge/herbaceous (89 and 55%) communities. Differences between estimated and field-observation mean values by land cover suggest other factors (e.g. climate, topography, shallow lithology) influence the distribution of NSP on a landscape scale. Furthermore, differences between mean field observation and estimated NSP probabilities were smallest when stratified by land cover in the Intermontane Boreal, as compared to other ecoregions in Alaska, suggesting stronger permafrost-vegetation linkages in this region. A detailed discussion of fire-permafrost interactions is not provided because model training data were limited for recent disturbances and is a topic of ongoing research efforts by the authors.

Land cover can serve as a proxy indicator for permafrost presence–absence because of vegetation's influence on surface energy balances and associations with soil characteristics (Jorgenson et al., 2013; Pastick, Rigge, et al., 2014; Shur & Jorgenson, 2007), consistent with field observations and model estimates in this study. Because deciduous and mixed forests are commonly associated with disturbances, south-facing slopes, thin organic layers and low soil moistures, soil thermal conductivities tend to be lower for these vegetation types (Jorgenson et al., 2010). Conversely, evergreen forests, shrub/scrub, and sedge tussock tundra are typically associated with thick organic layers and moist soils (Jorgenson et al., 2010; Pastick, Rigge, et al., 2014), both of which can serve as insulators to permafrost. Ecologically-driven or protected permafrost (i.e. discontinuous permafrost zone) is highly vulnerable to fire disturbances (Jorgenson et al., 2010), which are anticipated to increase in extent and severity in the future (Balshi et al., 2009). If burn severity levels and fire return intervals increase, NSP is likely to be profoundly impacted.

While topographical information was used only moderately within model development (Table A1), topography's influence on permafrost has been well documented. In this study, flat lowlands had higher and significantly different ($p < 0.001$) mean NSP probabilities than upland areas with higher slope gradients (estimated: 56% versus 35%; field observations: 32% versus 17%). NSP probabilities were inversely related to soil-wetness and slope, as derived by a digital elevation model, where mean estimated and field-observation NSP probabilities generally increased as soils became "wetter" or as slopes decreased. While aspect and elevation data were important in NSP model development, trends were not evident at the landscape scale.

Drainage and solar radiation are important factors controlling permafrost extents as these factors influence fauna, soil moisture, and hydrology (Hinkel & Nelson, 2003; Kreig & Reger, 1982; Riseborough et al., 2008; Shur & Jorgenson, 2007), consistent with field observations and model estimates in this study. Lowlands are commonly associated with areas of paludification and accumulations of thick surface organics because of impoundment of water on top of shallow permafrost (Kane, 1997). Uplands tend to have coarse, well-drained soils, which can lead to increased levels of thermal conductivity, reduced frozen and unfrozen conductivity ratios, and the absence of NSP. This finding corroborates analyses by Johnson et al. (2013) that show higher NSP in flat areas (43%) than on slopes >3.9% (35%) for the intermontane boreal. Areas with water accumulation may be hydrologically connected resulting in a thermal source, which can serve as a negative feedback to the permafrost system, consistent with field observations coinciding with surface water.

Shallow lithology was implicitly accounted for in our analyses, by use of topographical and spectral data, and is an important factor influencing permafrost properties and extents. While there are surficial geology maps available for the state, they often have poor spatial accuracies and no accompanying uncertainty estimates. In order to directly assess relations between NSP and shallow lithology, an additional analysis was conducted by stratifying NSP estimates by surficial deposit classes developed by, Jorgenson, Yoshikawa, et al. (2008) Despite being withheld from model development, mean estimated NSP probabilities varied nearly four-fold among surficial deposit types. Glaciomarine (97%), Eolian Sand (82%), Eolian Loess (69%), Alluvial-Marine (65%), and Colluvial-Hillside (59%) deposits held the highest mean NSP probabilities, and generally have fine-grained particle sizes and moderate to high ice contents. In contrast, Coastal and Bedrock deposits had the lowest mean NSP probabilities (21%) and are typically influenced by saline water or have low porosity. Intermediate classes consisted of fluvial or reworked deposits with moderate to large particle sizes. While Eolian Sand deposits had slightly higher NSP probabilities than Eolian Loess, this was due to differences in geographic location and size, and variations in climate–permafrost–ecosystem interactions. For example, in the intermontane boreal, NSP was found to be consistently lower in sandy soil textures (14%) than in other soil texture types (47%), regardless of topography (Johnson et al., 2013). Furthermore, because there were few high quality field data available for alpine soils (i.e. dry and rocky) and thaw depths are generally deeper than 1 m in these areas, our model tends to estimate these areas to be devoid of NSP.

3.3. Sensitivity of near-surface permafrost to climate-induced change

Future climate scenarios were applied to the calibrated NSP model to examine the model's response to long-term changes in climate under varying levels of severity during the 21st Century (Fig. 7). From 2010 to 2050, projected NSP extents declined by 7%, 14%, and 12% under low, moderate, and severe emission scenarios, respectively (Table 2). From 2010 to 2090, projected NSP areal extents declined by 16% to 24%. The greatest rate of predicted spatial change came during the 2010 to 2050 under the balanced A1B climate scenario. This time period corresponds to the A1B scenarios story of increased emissions in the first half of the century followed by suppressed emission levels because of increases in energy efficiency. Our model results indicate that NSP was more probable to degrade in arctic uplands (61% decrease in spatial frequency) than lowlands (19% decrease in spatial frequency) in the 21st Century, under the A1B scenario. Compared to other ecoregions, the predicted change in NSP in the arctic tundra decreased less (Fig. 8). However, this does not necessarily indicate that the arctic is less vulnerable to change than warmer areas such as the intermontane boreal. Because the ALT is typically thinner in the arctic than in the intermontane boreal, it is further from our 1-m depth for detecting NSP, thus requiring relatively more heat energy for permafrost to disappear over the same warming scenario. Spatial predictions of permafrost degradation were heterogeneous in nature but more pronounced for ecoregions in central Alaska where permafrost–vegetation–topographic interactions are more distinct (Figs. 3 and 7). The Bering Tundra ecoregion (i.e. Seward Peninsula) is projected by our model to undergo rapid NSP degradation in the first half of the 21st Century. Mountain Transitions and Intermontane Boreal ecoregions displayed slightly lower decreases in NSP extents during the 21st Century, ranging from 48 to 53%. During the first half of the 21st Century, model predictions indicated that NSP on uplands were more susceptible to change than NSP on lowlands of central regions of Alaska. However, lowland NSP distributions were projected to decrease more rapidly during the latter half of the 21st Century.

In comparison to other studies, our projected range of NSP disappearance (16 to 24%) corresponds well with the 22% loss of frozen ground in Alaska during the 21st Century predicted by Jafarov et al. (2012). Our projected reduction in permafrost extents are also comparable to the range (20.5–24.4%) for Canada in the 21st Century estimated by Zhang, Chen, and Riseborough (2008). As this is the first study to quantify the presence–absence of NSP in Alaska based on a large dataset of field observation, no direct-spatial comparisons can be made. Ground temperatures in northern Alaska have been reported to be increasing in recent years (Romanovsky, Smith, & Christiansen, 2010; Smith et al., 2010), consistent with projections of moderate NSP permafrost degradation in northern regions (Fig. 7). Moderate projections of NSP degradation in northern Alaska also aligns with 1-m depth temperature simulations carried out by Jafarov et al. (2012). Permafrost in the discontinuous permafrost zone is relatively warm and thus prone to permafrost degradation by climate warming (Osterkamp & Romanovsky, 1996; Shur & Jorgenson, 2007), consistent with model simulations of enhanced permafrost susceptibility in central regions of Alaska. Model simulations of rapid permafrost thaw in the Bering Tundra are consistent with recent observations of the degradation of thin discontinuous and continuous permafrost in the region (Hinzman et al., 2005; Yoshikawa & Hinzman, 2003). While ground temperatures are thought to be in disequilibrium with surface air temperatures, NSP is more likely to be in equilibrium with surface air temperatures than permafrost at depth (Zhang et al., 2008). Subsequently, our NSP projections are thought to represent close to equilibrium conditions. As our model was designed to estimate the presence–absence of permafrost within the top meter of the ground surface, projections of the change in permafrost extents at depth are not given. We also recognize the large uncertainty in the climate models, where the A1B assumes a perhaps unrealistic level of emission reductions, which is evident in that our projected decreases in permafrost are much less in the second half of the century compared to the first half.

Lowland areas with organic-rich soils and moderate to high ground-ice contents were estimated to account for 4.5% of the study domain, and are particularly susceptible to thermokarst development and ground subsidence. Our estimate of area predisposed to lowland thermokarst is similar to interpretations made by Jorgenson, Shur, et al. (2008), where 4.4% of the Alaskan discontinuous permafrost

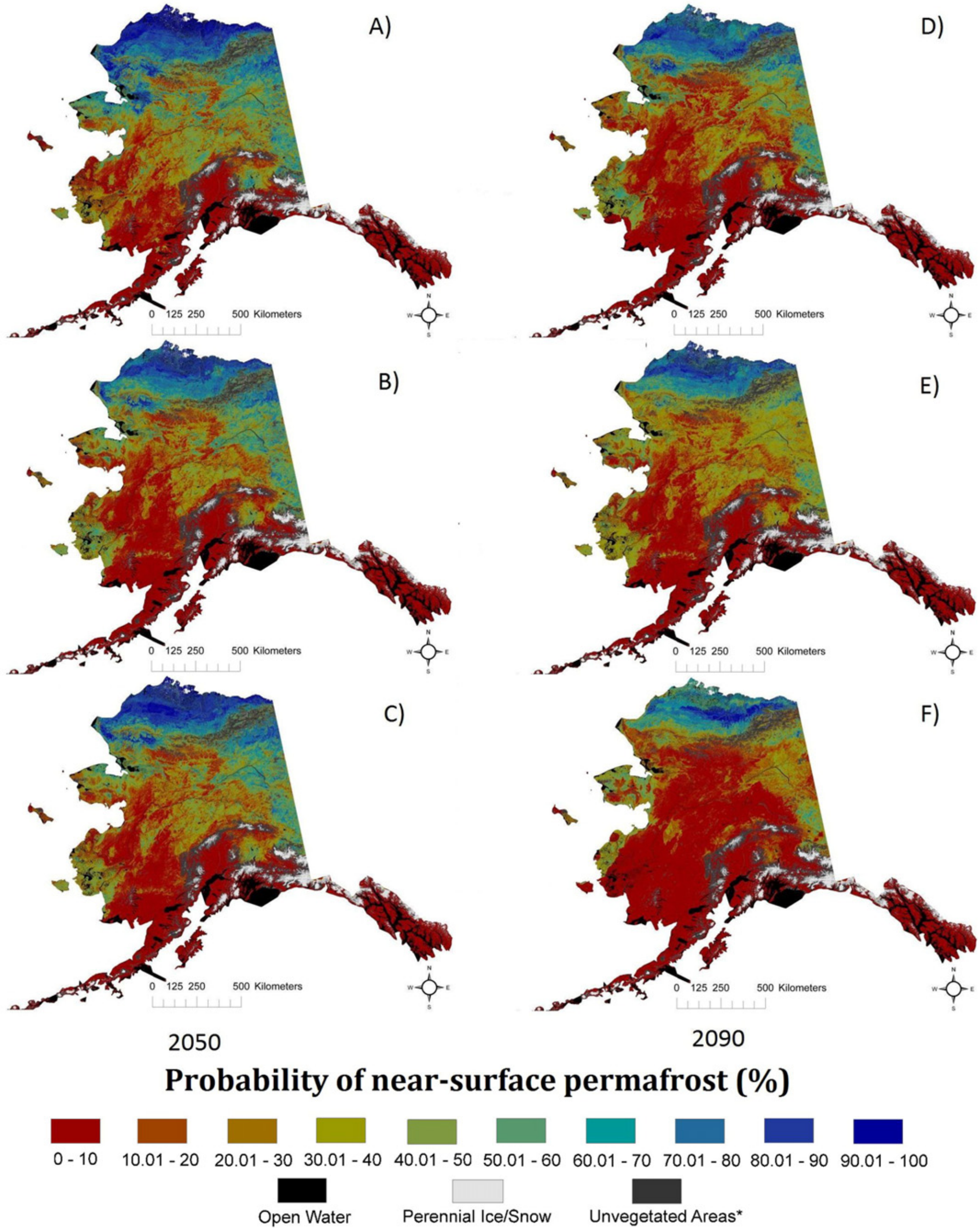

Fig. 7. Projected near-surface (within 1 m) permafrost probabilities for Alaska, using downscaled climate forcing data from an average of five general circulation model outputs (i.e. cccma_cgcm31, gfdl_cm2_1, miroc3_2_medres, mpi_echam5, ukmo_hadcm3) with B1, A1B, and A2 emission scenarios for the 21st Century as follows: (a) B1 — 2050; (b) A1B — 2050; (c) A2 — 2050; (d) b1 — 2090; (e) A1B — 2090, and; (f) A2 — 2090.

Table 2
Percentage area predicted to be underlain or devoid of near-surface (within 1 m) permafrost (NSP) for Alaska using downscaled climate forcing data from an average of five general circulation model outputs (i.e. cccma_cgcm31, gfdl_cm2_1, miroc3_2_medres, mpi_echam5, ukmo_hadcm3) with B1, A1B, and A2 emission scenarios for the 21st Century. Masked areas represent areas commonly devoid or underlain by NSP and are composed of open water, barren land, perennial ice/snow, and cultivated land covers as depicted by the 2001 National Land Cover Database (Homer et al., 2007).

	% Absent	% Present	% Masked
Base line — 2010	44%	34%	22%
B1 — 2050	51%	27%	22%
A1B — 2050	58%	20%	22%
A2 — 2050	56%	22%	22%
B1 — 2090	60%	18%	22%
A1B — 2090	66%	12%	22%
A2 — 2090	68%	10%	22%

zone had lowland thermokarst features. In our study, approximately 94% of the predisposed areas are predicted to experience NSP disappearance by the end of 21st Century (under the A1B emission scenario). There are large stores of frozen soil carbon in these areas, it is estimated that the frozen soil carbon content is about 76 Mg C ha^{-1} or 1.1 Pg C, according to one study (Wylie et al., in press). All areas projected to undergo disappearance of NSP (under the A1B emission scenario), have been estimated to contain, on average, 51 Mg C ha^{-1} of frozen soil carbon or 30% (3.4 Pg C) of the estimated permafrost C pools of Alaska (Wylie et al., in press). Thus, these areas could potentially remobilize large amounts of soil carbon upon permafrost thaw. Because we did not explicitly account for differences in permafrost C at depth and large uncertainties in frozen C stock estimates exist, and because only a small proportion of the C is likely to be mineralized (Schuur et al., 2015), vulnerable frozen C should not be viewed as the total amount of C that will

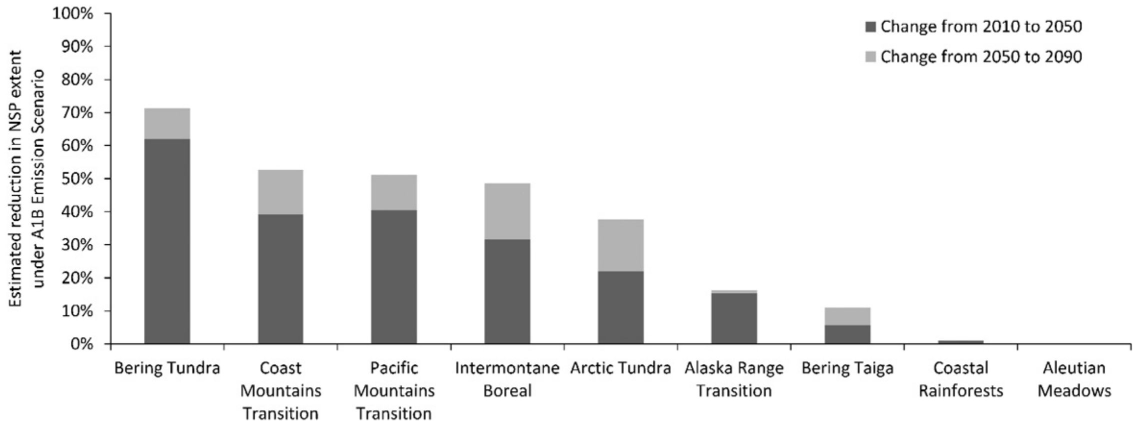

Fig. 8. Estimated decreases in near-surface (within 1 m) permafrost extent by ecoregion (Nowacki et al., 2001) under the A1B emission scenario for the 21st Century.

be released due to thaw. As additional frozen soil carbon estimates become available, which better capture the spatial and vertical distributions of C, these estimates can be incorporated into our approach to identify ecosystem properties that are susceptible to climate-induced permafrost thaw.

As permafrost thaws, soils can become drier and more susceptible to combustion by wildfire (Harden et al., 2010), and ground subsidence and water impoundment can alter ecological succession patterns and the distribution of peatlands (Quinton, Hayashi, & Chasmer, 2009). Such changes could influence local topography, thermal and hydraulic properties in the subsurface (Riseborough et al., 2008), which have been assumed to remain unchanged under future climates. The future impacts of disturbance-induced change to permafrost are particularly difficult to quantify because we do not know where and when future disturbances will occur, and the effects of disturbance on permafrost vary as a function of time, burn severity, vegetation succession, and climate conditions (Nossov et al., 2013; Yoshikawa, Bolton, et al., 2003). Changes in vegetation characteristics and micro-topography can also influence permafrost systems, but future projections of these changes currently are not available or are generalized. The lack of information on projected changes in surface conditions (e.g. vegetation, organic layer thickness, topography, fire and other disturbances) has resulted in projections of permafrost dynamics being largely forced by regional or global climate model data (Bonnaventure & Lewkowicz, 2013; Jafarov et al., 2012; Lawrence & Slater, 2005; Mishra & Riley, 2014), as is the case in our sensitivity analyses. Subsequently, projections of future response of NSP to climate warming that do not account for dynamically changing surface properties related to precipitation, disturbance, vegetation, hydrology, and soils should be viewed as highly uncertain. We acknowledge recent efforts aimed at coupling the Dynamic Organic Soil Terrestrial Ecosystem Model (DOS-TEM) and Alaska Frame-Based Ecosystem Code (ALFRESCO) model to understand permafrost–fire interactions (e.g. Genet et al., 2013), but this approach is conducted at a 1-km resolution, makes large simplifying assumptions about terrain complexity, and predictions have been shown to overestimate ALT under current climates (Wylie et al., in press). From the discussion above, it is apparent that more work and data are needed to better understand the vulnerability and resilience of permafrost-affected soils to climate and disturbance-induced change.

4. Conclusion

We used a decision and regression tree modeling approach to statistically and spatially extend field observations of permafrost properties throughout Alaska with explicit probabilities and uncertainties. Our data fusion approach was able to generate moderate-resolution (30-m pixels) maps of near-surface (within 1 m) permafrost, active-layer thickness, and associated uncertainty estimates throughout most of Alaska. This approach has the advantage of incorporating large sets of highly spatially variable properties, unlike thermal physical modeling, which extrapolates mean values for many properties over large areas. Map accuracies were assessed using independent field observations and cross-validation techniques, and demonstrate that our approach is suitable for predicting permafrost properties in the near surface. Using the calibrated model, we project near-surface permafrost will disappear on 16 to 24% of the area in Alaska and will be present on only 10 to 18% of the land in Alaska at the end of the 21st Century based on climate projections involving low (B1), moderate (A1B) and severe (A2) emission scenarios. Recently created frozen soil carbon maps and future permafrost projections indicate that a substantial portion of the permafrost C pool of Alaska may be vulnerable to climate-induced permafrost thaw (under moderate emission scenarios). Because the current model is designed to estimate near-surface (within 1 m) permafrost, and not permafrost at depth, areas identified to be absent or projected to undergo near-surface permafrost degradation may contain permafrost below 1 m. Potential decreases in permafrost extent and the frozen status of soil C may be underestimated because future projections did not account for future disturbance impacts. Simulations suggest that the central region of Alaska is more vulnerable to near-surface permafrost degradation than more northerly regions. Projections of near-surface permafrost degradation were more pronounced in upland ecosystems compared to lowland ecosystems in first half of the 21st Century. Conversely, near-surface permafrost degradation was estimated to increase in lowland ecosystems in the second half of the 21st Century. We caution that the dynamic changes in fire regimes, hydrology, vegetation, soils, and feedbacks associated with permafrost responses to climate warming limit the validity of this modeling approach, which assumes static surface conditions. This study demonstrates that, when taken together, field observations, climatic data, remotely sensed and mapped biophysical properties, and empirical modeling can help advance the current state of knowledge of permafrost landscapes.

Acknowledgments

Research was funded by the U.S. Geological Survey (USGS) Land Change Science Program. Work was performed under USGS contract G08PC91508. We thank 3 anonymous reviewers and Burke Minsley (USGS) for constructive comments that enhanced this manuscript.

Any use of trade, firm, or product names is for descriptive purposes only and does not imply endorsement by the U.S. Government.

Appendix A

Table A1
Predictor usage or predictor importance was defined as the number of training cases for which the value of the environmental predictor is used in predicting the presence–absence of near-surface (within 1 m) permafrost (NSP), divided by the total number of training cases in the model development database.

	Environmental predictors	Presence–absence of NSP
		Predictor usage (%)
Topography	Elevation	54
	Aspect	36
	Percent Slope	–
	Compound topographic index	65
	Potential incident radiation	–
Vegetation and land surface characteristics	Land cover	67
	Wetlands (Whitcomb et al., 2009)	–
	Landsat — band 1	63
	Landsat — band 2	–
	Landsat — band 3	–
	Landsat — band 4	100
	Landsat — band 5	–
	Landsat — band 7	54
	NDVI (normalized difference vegetation index)	54
	SAVI (soil-adjusted vegetation index)	–
	gNDVI (green normalized vegetation index)	47
	EVI (enhanced vegetation index)	–
	NDII (normalized difference infrared index)	70
	NDII7 (normalized difference infrared index band 7)	80
	NDWI (normalized difference water index)	63
	NDWI7 (normalized difference water index band 7)	–
	Spatial variation — coefficient of variation (Landsat bands 3, 4, and 5)	68
Climate	Mean annual air temperature[a]	100
	Mean annual precipitation[a]	100
	Mean summer precipitation[a]	–
	Mean winter precipitation[a]	100
	Mean day of thaw[a]	100
	Mean day of freeze[a]	73
	Mean length of growing season[a]	69

[a] Indicates data obtained from Scenario Network for Alaska and Arctic Planning (http://www.snap.uaf.edu/).

References

Anisimov, O. A., & Nelson, F. E. (1997). Permafrost zonation and climatic change in the northern hemisphere: Results from transient general circulation models. *Climatic Change*, *35*, 241–258.

Balshi, M. S., McGuire, A. D., Duffy, P., Flannigan, M., Kicklighter, D. W., & Melillo, J. (2009). Vulnerability of carbon storage in North American boreal forests to wildfires during the 21st century. *Global Change Biology*, *15*, 1491–1510.

Barrett, K., McGuire, A. D., Hoy, E. E., & Kasischke, E. S. (2011). Potential shifts in dominant forest cover in interior Alaska driven by variations in fire severity. *Ecological Applications*, *21*, 2380–2396.

Beck, P. S. A., & Goetz, S. J. (2011). Satellite observations of high northern latitude vegetation productivity changes between 1982 and 2008: Ecological variability and regional differences. *Environmental Research Letters*, *6*, 04550.

Belshe, E. F., Schuur, E. A. G., & Grosse, G. (2013). Quantification of upland thermokarst features with high resolution remote sensing. *Environment Researcher Letters*, *8*, 035016. http://dx.doi.org/10.1088/1748.

Bonnaventure, P. P., & Lewkowicz, A. G. (2013). Impacts of mean annual air temperature change on a regional permafrost probability model for the southern Yukon and northern British Columbia, Canada. *The Cryosphere*, *7*, 935–946. http://dx.doi.org/10.5194/tc-7-935-2013.

Bonnaventure, P. P., Lewkowicz, A. G., Kremer, M., & Sawada, M. C. (2012). A permafrost probability model for the southern Yukon and northern British Columbia, Canada. *Permafrost and Periglacial Processes*, *23*, 52–68. http://dx.doi.org/10.1002/ppp.1733.

Brown, J., Ferrians, O. J., Heginbottom, J. A., & Melnikov, E. S. (1997). *Circum-Arctic map of permafrost and ground ice conditions*. U.S. Geological Survey, Reston, Virginia. CP-45.

Brown, J. E., & Pewe, T. L. (1973). Distribution of permafrost in North America and its relationship to the environment. *Cl. Review, 1963–1973 "Permafrost" Second International Conference, National Academy of Sciences. Washington* (pp. 15–21).

Chapin, F. S., III, Mcguire, A. D., Randerson, J., Pielke, R., Baldocchi, D., et al. (2000). Arctic and boreal ecosystems of western North America as components of the climate system. *Global Change Biology*, *6*, 211–223.

Clark, M. H., & Duffy, M. S. (2003). *Soil survey of Denali National Park Area, Alaska*. Palmer, AK: Natural Resource Conservation Service (822 pp.).

Congalton, R. G. (1991). A review of assessing the accuracy of classifications of remotely sensed data. *Remote Sensing of Environment*, *37*, 35–46.

Duguay, C. R., Zhang, T., Leverington, D. W., & Romanovsky, V. E. (2005). Satellite remote sensing of permafrost and seasonally frozen ground. In C. R. Duguay, & A. Pietroniro (Eds.), *Remote Sensing in Northern Hydrology: Measuring Environmental Change. Geophysical Monographs Series*, *vol. 163*, . Washington, DC: American Geophysical Union.

Freund, Y., & Schapire, R. (1996). Experiments with a new boosting algorithm. *Machine Learning: Proceedings of the Thirteenth International Conference* (pp. 148–156). San Francisco: Morgan Kauffman.

Friedl, M. A., & Brodley, C. E. (1997). Decision tree classification of land cover from remotely sensed data. *Remote Sensing of Environment*, *61*, 399–409.

Gangodagamage, C., Rowland, J. C., Hubbard, S. S., Brumby, S. P., Liljedahl, A. K., Wainwright, H., et al. (2014). Extrapolating active layer thickness measurements across Arctic polygonal terrain using LiDAR and NDVI data sets. *Water Resources Research*, *50*, 6339–6357. http://dx.doi.org/10.1002/2013WR014283.

Genet, H., McGuire, A. D., Barrett, K., Breen, A., Euskirchen, E. S., Johnstone, J. F., et al. (2013). Modeling the effects of fire severity and climate warming on active layer thickness and soil carbon storage of black spruce forests across the landscape in interior Alaska. *Environmental Research Letters*, *8*(4), 04501.

Gesch, D., Oimoen, M., Greenlee, S., Nelson, C., Steuck, M., & Tyler, D. (2002). The national elevation dataset. *Photogrammetric Engineering and Remote Sensing*, *68*, 5–11.

Gessler, P. E., Moore, I. D., McKenzie, N. J., & Ryan, P. J. (1995). Soil-landscape modeling and spatial prediction of soil attributes. *International Journal of GIS*, *9*(4), 421–432.

Grosse, G., et al. (2011). Vulnerability of high-latitude soil organic carbon in North America to disturbance. *Journal of Geophysical Research*, *116*, G00K06. http://dx.doi.org/10.1029/2010JG001507.

Hall, D. K. (1982). A review of the utility of remote sensing in Alaskan permafrost studies. *IEEE Transactions on Geoscience and Remote Sensing*, *GE-20*(390–394).

Hall, M. A. (2000). Correlation-based feature selection for discrete and numeric class machine learning. *Proc. 17th Int', l Conf. Machine Learning* (pp. 359–366).

Hall, D. K., Ormsby, J. P., Johnson, L., & Brown, J. (1980). Landsat digital analysis of the initial recovery of burned tundra at Kokolik River, Alaska. *Remote Sensing of Environment*, *10*, 263–272. http://dx.doi.org/10.1016/0034-4257(80)90086-3.

Harden, J. W., Koven, C. D., Ping, C., Hugelius, G., McGuire, A., Camill, P., et al. (2010). Field information links permafrost carbon to physical vulnerabilities of thawing. *Geophysical Research Letters*, *39*(15), L15704. http://dx.doi.org/10.1029/2012GL051958.

Hastie, T., Tibshirani, R., & Friedman, J. H. (2009). *The elements of statistical learning: Data mining, inference and prediction* (2nd ed.). New York, USA: Springer, 533.

Hinkel, K. M., & Nelson, F. E. (2003). Spatial and temporal patterns of active layer thickness at Circumpolar Active Layer Monitoring (CALM) sites in northern Alaska, 1995–2000. *Journal of Geophysical Research — Atmospheres*, *108*(D2) (pp. ALT 9 - 1 ALT 9 - 13).

Hinzman, L. D., et al. (2005). Evidence and implications of recent climate change in northern Alaska and other arctic regions. *Climatic Change*, *72*, 251–298.

Hoelzle, M., Mittaz, C., Eztelmuller, B., & Haeberli, W. (2001). Surface energy fluxes and distribution models relating permafrost in European Mountain areas: An overview of current developments. *Permafrost and Periglacial Processes*, *12*(1), 53–68.

Homer, C., Dewitz, J., Fry, J., Coan, M., Hossain, N., Larson, C., et al. (2007). Completion of the 2001 National Land Cover Database for the Conterminous United States. *Photogrammetric Engineering and Remote Sensing*, *73*(4), 337–341.

IPCC (2007). Climate change 2007: The physical science basis. *Contribution of Working Group I to the Fourth Assessment Report of the Intergovernmental Panel on Climate Change*. Cambridge, United Kingdom and New York, NY, USA: Cambridge University Press.

IPCC (2013). Climate change 2013: The physical science basis. *Contribution of Working Group I to the Fifth Assessment Report of the Intergovernmental Panel on Climate Change*. Cambridge, United Kingdom and New York, NY, USA: Cambridge University Press (1535 pp.).

Jafarov, E. E., Marchenko, S. S., & Romanovsky, V. E. (2012). Numerical modeling of permafrost dynamics in Alaska using a high spatial resolution dataset. *The Cryosphere*, *6*, 613–624.

Jelinksi, N. A. (2014). Cryoturbation in the Central Brooks Range, Alaska. *Soil Horizon*. http://dx.doi.org/10.2136/sh13-01-0006.

Ji, L., Wylie, B. K., Nossov, D. R., Peterson, B., Waldrop, M. P., McFarland, J. W., et al. (2012). Estimating aboveground biomass in interior Alaska with Landsat data and field measurements. *International Journal of Applied Earth Observation and Geoinformation*, *18*, 451–461.

Jiang, Y., Rocha, A. V., O'Donnell, J. A., Drysdale, J. A., Rastetter, E. B., Shaver, G. R., et al. (2015). Contrasting soil thermal responses to fire in Alaskan tundra and boreal forest. *Journal of Geophysical Research — Earth Surface*, *120*, 363–378. http://dx.doi.org/10.1002/2014JF003180.

Johansson, M., Callaghan, T. V., Julia, B., Akerman, H. J., Jackowicz-Korczynski, M., & Christensen, T. R. (2013). Rapid responses of permafrost and vegetation to experimentally increased snow cover in sub-arctic Sweden. *Environmental Research Letters*. http://dx.doi.org/10.1088/1748-9326/8/3/035025.

Johnson, K. D., Harden, J., McGuire, A. D., Clark, M., Yuan, F., & Finley, O. A. (2013). Permafrost and organic layer interactions over a climate gradient in a discontinuous permafrost zone. *Environmental Research Letters*. http://dx.doi.org/10.1088/1748-9326/8/3/035028.

Jorgenson, T., Harden, J., Kanevskiy, M., O'Donnell, J., Wickland, K., Ewing, S., et al. (2013). Reorganization of vegetation, hydrology and soil carbon after permafrost degradation across heterogeneous boreal landscapes. *Environmental Research Letters*, *8*, 035017.

Jorgenson, M. T., Kanevskiy, M., Shur, Y., Grunblatt, J., Ping, C. L., & Michaelson, G. (2014). Permafrost database development, characterization, and mapping for northern Alaska. *Report for Arctic Landscape Conservation Cooperative by Alaska Ecoscience and University of Alaska Fairbanks* (45 pp. http://www.gina.alaska.edu/projects/permafrost-database-and-maps-for-northern-alaska).

Jorgenson, M. T., Racine, C. H., Walters, J. C., & Osterkamp, T. E. (2001). Permafrost degradation and ecological changes associated with a warming climate in central Alaska. *Climatic Change*, *48*, 551–579. http://dx.doi.org/10.1023/A:1005667424292.

Jorgenson, M. T., Romanovsky, V., Harden, J., Shur, Y., O'Donnell, J., Schuur, E. A. G., et al. (2010). Resilience and vulnerability of permafrost to climate change. *Canadian Journal of Forest Research*, *40*(7).

Jorgenson, M. T., Roth, J. E., Raynolds, M., Smith, M. D., Lentz, W., Zusi-Cobb, L., et al. (1999). An ecological land survey for Fort Wainwright, Alaska. *CRREL Report 99-9*. Hanover, NH: U.S. Army Cold Regions Research and Engineering Laboratory (83 pp.).

Jorgenson, M. T., Roth, J. E., Smith, M. D., Schlentner, S., Lentz, W., Pullman, E. R., et al. (2001). *An ecological land survey for Fort Greely, Alaska*. Hanover, NH: U.S. Army Cold Regions Research and Engineering Laboratory (ERDC/CRREL TR-01-04., 85 pp.).

Jorgenson, M. T., Shur, Y., & Osterkamp, T. E. (2008). Thermokarst in Alaska. *Proceedings of the Ninth International Conference on Permafrost* (8 pp.).

Jorgenson, M. T., Shur, Y. L., & Pullman, E. R. (2006). Abrupt increase in permafrost degradation in Arctic Alaska. *Geophysical Research Letters*, *33*, L02503. http://dx.doi.org/10.1029/2005GL024960.

Jorgenson, M. T., Yoshikawa, K., Kanveskiy, M., Shur, Y., Romanovsky, V., Marchenko, S., et al. (2008). In D. L. Kane, & K. M. Hinkel (Eds.), *Permafrost characteristics of Alaska Ninth International Conference on Permafrost Extended Abstracts* (pp. 121–122). Fairbanks: University of Alaska.

Kääb, A. (2008). Remote sensing of permafrost-related problems and hazards. *Permafrost and Periglacial Processes*, *19*(2), 107–136.

Kane, D. L. (1997). The impact of hydrologic perturbations on arctic ecosystems induced by climate change. In W. C. Oechel, T. Callaghan, T. Gilmanov, J. I. Holten, B. Maxwell, U. Molau, & B. Sveinbjornsson (Eds.), *Global Change and Arctic Terrestrial Ecosystems* (pp. 63–81). New York: Springer.

Keyser, A. R., Kimball, J. S., Nemani, R. R., & Running, S. W. (2000). Simulating the effects of climate change on the carbon balance of North American high latitude forests. *Global Change Biology*, *6*, 185–195.

Kreig, R. A., & Reger, R. D. (1982). Air-photo analysis and summary of landform soil properties along the route of the Trans-Alaska Pipeline System. *Alaska Div. of Geol. and Geophys. Surv., Fairbanks. Geol. Rep.*, *66*, (149 pp.).

Laidler, G. J., & Treitz, P. (2003). Biophysical remote sensing of arctic environments. *Progress in Physical Geography*, *27*, 44–68. http://dx.doi.org/10.1191/0309133303pp358ra.

Lara, M. J., McGuire, A. D., Euskirchen, E. S., Tweedie, C. E., Hinkel, K. M., Skurikhin, A. N., et al. (2015). Polygonal tundra geomorphological change in response to warming alters future CO_2 and CH_4 flux on the Barrow Peninsula. *Global Change Biology*, *21*, 1634–1651. http://dx.doi.org/10.1111/gcb.12757.

Larsen, P. H., Goldsmith, S., Smith, O., Wilson, M. L., Strzepek, K., Chinowsky, P., et al. (2008). Estimating future costs for Alaska public infrastructure at risk from climate change. *Global Environmental Change*, *18*, 442–457.

Lawrence, D. M., & Slater, A. G. (2005). A projection of severe near-surface permafrost degradation during the 21st century. *Geophysical Research Letters*, *32*, L24401. http://dx.doi.org/10.1029/2005GL025080.

Leverington, D. W., & Duguay, C. R. (1996). Evaluation of three supervised classifiers in mapping 'depth to late-summer frozen ground', central Yukon Territory. *Canadian Journal of Remote Sensing*, *22*, 163–174.

Leverington, D. W., & Duguay, C. R. (1997). A neural network method to determine the presence or absence of permafrost near Mayo, Yukon Territory, Canada. *Permafrost and Periglacial Processes*, *8*, 205–215.

Lewkowicz, A. G., & Duguay, C. R. (1999). Detection of permafrost features using SPOT Panchromatic Imagery, Fosheim Peninsula, Ellesmere Island, N.W.T. *Canadian Journal of Remote Sensing*, *25*, 34–44.

Marchenko, S., Romanovsky, V., & Tipenko, G. (2008). Numerical modeling of spatial permafrost dynamics in Alaska. *Proceedings of the Eighth International Conference on Permafrost* (pp. 190–204). Fairbanks: Willey, Institute of Northern Engineering, University of Alaska.

Martin, M. P., Wattenbach, M., Smith, P., Meersmans, J., Jolivet, C., Bouloone, L., et al. (2011). Spatial distribution of soil organic carbon stocks in France. *Biogeosciences*, *8*, 1053–1065.

McCune, B., & Keon, D. (2002). Equations for potential annual direct incident radiation and heat load. *Journal of Vegetation Science*, *13*, 603–606. http://dx.doi.org/10.1111/j.1654-1103.2002.tb02087.x.

McMichael, C. E., Hope, A. S., Stow, D. A., & Fleming, J. B. (1997). The relation between active layer depth and a spectral vegetation index in arctic tundra landscapes of the North Slope of Alaska. *International Journal of Remote Sensing*, *18*(11), 2371–2382.

Mishra, M., & Riley, W. J. (2014). Active-layer thickness across Alaska: Comparing observation-based estimates with CMIP5 earth system model predictions. *Soil Science Society of America Journal*, *78*, 894–902. http://dx.doi.org/10.2136/sssaj2013.11.0484.

Morrissey, L. A., Strong, L., & Card, D. H. (1986). Mapping permafrost in the boreal forest with thematic mapper satellite data. *Photogrammetric Engineering and Remote Sensing*, *52*, 1513–1520.

Myneni, R. B., Keeling, C. D., Tucker, C. J., Asrar, G., & Nemani, R. R. (1997). Increased plant growth in the northern high latitudes from 1981 to 1991. *Nature*, *386*, 698–702.

National Research Council (2014). *Opportunities to use remote sensing in understanding permafrost and related ecological characteristics: Report of a workshop*. Washington, DC: The National Academies Press.

Nauta, A. L., Heijmans, M. P. D., Blok, D., Limpens, J., Elberling, B., Gallagher, A., et al. (2015). Permafrost collapse after shrub removal shifts tundra ecosystem to a methane source. *Nature Climate Change*, *5*, 67–70. http://dx.doi.org/10.1038/NCLIMATE2446.

Nelson, F. E., Shiklomanov, N. I., Mueller, G. R., Hinkel, K. M., Walker, D. A., & Bockheim, J. G. (1997). Estimating active-layer thickness over a large region: Kuparuk River Basin, Alaska, USA. *Arctic and Alpine Research*, *29*, 367–378.

Nguyen, T. -N., Burn, C. R., King, D. J., & Smith, S. L. (2009). Estimating the extent of near-surface permafrost using remote sensing, Mackenzie Delta, Northwest Territories. *Permafrost and Periglacial Processes*, *20*, 141–153. http://dx.doi.org/10.1002/ppp.637.

Nossov, D. R., Jorgenson, M. T., Kielland, K., & Kanevskiy, M. Z. (2013). Edaphic and microclimatic controls over permafrost response to fire in interior, Alaska. *Environmental Research Letters*, *8*, 035013. http://dx.doi.org/10.1088/1748-9326/8/3/035013.

Nowacki, G., Spencer, P., Brock, T., Fleming, M., & Jorgenson, T. (2001). Unified ecoregions of Alaska and neighboring territories. *US Geological Survey Open-File Report 02-297*. Anchorage, Alaska, USA: US Geological Survey.

Osterkamp, T. E., Jorgenson, M. T., Schuur, E. A. G., Shur, Y. L., Kanevsky, M. Z., Vogel, J. G., et al. (2009). Physical and ecological changes associated with warming permafrost and thermokarst in Interior Alaska. *Permafrost and Periglacial Processes*, *20*, 235–256.

Osterkamp, T. E., & Romanovsky, V. E. (1996). Characteristics of changing permafrost temperatures in the Alaskan Arctic, USA. *Arctic and Alpine Research*, *28*(3), 267–273.

Panda, S. K., Marchenko, S. S., & Romanovsky, V. E. (2014a). *High-resolution permafrost modeling in Wrangell-St. Elias National Park and Preserve*. National Park Service, 1–40 (NPS/CAKN/NRTR-2014/861).

Panda, S. K., Marchenko, S. S., & Romanovsky, V. E. (2014b). *High-resolution permafrost modeling in Denali National Park and Preserve*. National Park Service, 1–46 (NPS/CAKN/NRTR-2014/858).

Panda, S. K., Prakash, A., Jorgenson, M. T., & Solie, D. N. (2012). Near-surface permafrost distribution mapping using logistic regression and remote sensing in Interior Alaska. *GIScience and Remote Sensing*, *49*, 346–363.

Panda, S. K., Prakash, A., Solie, D. N., Romanovsky, V. E., & Jorgenson, M. T. (2010). Remote sensing and field-based mapping of permafrost distribution along the Alaska Highway corridor, Interior Alaska. *Permafrost and Periglacial Processes*, *21*, 271–281.

Pastick, N. J., Jorgenson, M. T., Wylie, B. K., Minsley, B. J., Ji, L., Walvoord, M. A., et al. (2013). Extending airborne electromagnetic surveys for regional active layer and permafrost mapping with remote sensing and ancillary data, Yukon Flats Ecoregion, Central Alaska. *Permafrost and Periglacial Processes*, *24*, 184–199. http://dx.doi.org/10.1002/ppp.1775.

Pastick, N. J., Jorgenson, M. T., Wylie, B. K., Rose, J. R., Rigge, M., & Walvoord, M. A. (2014). Spatial variability and landscape controls of near-surface permafrost within the Alaskan Yukon River Basin. *Journal of Geophysical Research — Biogeosciences*, *119*, 1244–1265. http://dx.doi.org/10.1002/2013JG002594.

Pastick, N. J., Rigge, M., Wylie, B. K., Jorgenson, M. T., Rose, J. R., Johnson, K. D., et al. (2014). Distribution and landscape controls of organic layer thickness and carbon within the Alaskan Yukon River Basin. *Geoderma*, *230–231*, 79–94.

Pearson, R. G., Phillips, S. J., Loranty, M. M., Beck, P. S. A., Damoulas, T., Knight, S. J., et al. (2013). Shifts in Arctic vegetation and associated feedbacks under climate change. *Nature Climate Change*, *3*, 673–677.

Peddle, D. R., Foody, G. M., Zhang, A., Franklin, S. E., & Ledrew, E. F. (1994). Multisource image classification II: An empirical comparison of evidential reasoning, linear discriminant analysis, and maximum likelihood algorithms for alpine land cover classification. *Canadian Journal of Remote Sensing*, *20*, 397–408.

Peddle, D. R., & Franklin, S. E. (1993). Classification of permafrost active layer depth from remotely sensed and topographic evidence. *Remote Sensing of Environment*, *44*, 67–80.

Perlich, C., Provost, F., & Simonoff, J. S. (2003). Tree-induction vs. logistic regression: A learning curve analysis. *Journal of Machine Learning Research*, *4*, 211–255.

Quinlan, R. (1993). *C4.5: Programs for machine learning*. San Mateo: Morgan Kaufmann.

Quinlan, R. (1996). Bagging, boosting, and C4.5. *Proceedings, Fourteenth National Conference on Artificial Intelligence*.

Quinlan, J. R. (2003). See5: An informal tutorial. http://www.rulequest.com/see5-win.html (20 April 2014)

Quinton, W. L., Hayashi, M., & Chasmer, L. (2009). Peatland hydrology of discontinuous Permafrost in the Northwest Territories: overview and synthesis. *Canadian Water Resources Journal*, *34*, 311–328.

Raynolds, M. K., & Walker, D. A. (2008, June). Circumpolar relationships between permafrost characteristics, NDVI, and arctic vegetation types. *Ninth International Conference on Permafrost. Fairbanks, AK*.

Riseborough, D., Shiklomanov, N., Etzelmüller, B., Gruber, S., & Marchenko, S. (2008). Recent advances in permafrost modelling. *Permafrost and Periglacial Processes*, *19*, 137–156. http://dx.doi.org/10.1002/ppp.615.

Rogers, B. M., Veraverbeke, S., Azzari, G., Czimczik, C. I., Holden, S. R., Mouteva, G. O., et al. (2014). Quantifying fire-wide carbon emissions in interior Alaska using field measurements and Landsat imagery. *Journal of Geophysical Research — Biogeosciences*, *119*, 1608–1629. http://dx.doi.org/10.1002/2014JG002657.

Romanovsky, V., & Cable, W. (2014). Establishing a distributed permafrost observation network in Western Alaska. *Western Alaska Landscape Conservation Cooperative Project 2014 Final Performance Report* (34 pp.).

Romanovsky, E. E., Smith, S. L., & Christiansen, H. H. (2010). Permafrost thermal state in the polar Northern Hemisphere during the international polar year 2007–2009: A synthesis. *Permafrost and Periglacial Processes*, *21*, 106–116. http://dx.doi.org/10.1002/ppp.689.

Schaefer, K., Lantuit, H., Romanovsky, V. E., Schuur, E. A. G., & Witt, R. (2014). The impact of the permafrost carbon feedback on global climate. *Environmental Research Letters*, *9*(8), 1–9.

Schuur, E. A. G., et al. (2008). Vulnerability of permafrost carbon to climate change: Implications for the global carbon cycle. *BioScience*, *58*, 701–714. http://dx.doi.org/10.1641/B580807.

Schuur, E. A. G., et al. (2015). Climate change and the permafrost carbon feedback. *Nature*, *520*, 171–179. http://dx.doi.org/10.1038/nature14338.

Shur, Y. L., & Jorgenson, M. T. (2007). Patterns of permafrost formation and degradation in relation to climate and ecosystems. *Permafrost and Periglacial Processes*, *18*, 7–19. http://dx.doi.org/10.1002/ppp.582.

Smith, S. L., & Burgess, M. M. (2004). Sensitivity of permafrost to climate warming in Canada. *Geological Survey of Canada Bulletin*, *579* (24 pp.).

Smith, S. L., Romanovsky, V. E., Lewkowicz, A. G., Burn, C. R., Allard, M., Clow, G. D., et al. (2010). Thermal state of permafrost in North America — A contribution to the international polar year. *Permafrost and Periglacial Processes*, *21*, 117–135.

Stieglitz, M., Déry, S. J., Romanovsky, V. E., & Osterkamp, T. E. (2003). The role of snow cover in the warming of the arctic permafrost. *Geophysical Research Letters*, *30*(13), 1721. http://dx.doi.org/10.1029/2003GL017337.

Stow, D. A., Hope, A., McGuire, D., et al. (2004). Remote sensing of vegetation and land-cover change in arctic tundra ecosystems. *Remote Sensing of Environment*, *89*, 281–308.

Swanson, D. K. (2012). *Vegetation sampling in the Arctic inventory and monitoring network, 2009–2012.* Natural Resource Data Series NPS/ARCN/NRDS — 2012/408. Fort Collins, Colorado: National Park Service.

Veraverbeke, S., Gitas, I., Katagis, T., Polychronaki, A., Somers, B., & Goossens, R. (2012). Assessing post-fire vegetation recovery using red-near infrared vegetation indices: Accounting for background and vegetation variability. *ISPRS Journal of Photogrammetry and Remote Sensing*, *68*, 28–39.

Wainwright, H. M., Dafflon, B., Smith, L. J., Hahn, M. S., Curtis, J. B., Wu, Y., et al. (2015). Identifying multiscale zonation and assessing the relative importance of polygon geomorphology on carbon fluxes in an Arctic Tundra Ecosystem. *Journal of Geophysical Research — Biogeosciences*, *120*. http://dx.doi.org/10.1002/2014JG002799.

Walsh, J. E., Chapman, W. L., Romanovsky, V., Christensen, J. H., & Stendel, M. (2008). Global climate model performance over Alaska and Greenland. *Journal of Climate*, *21*, 6156–6174.

Walvoord, M. A., & Striegl, R. G. (2007). Increased groundwater to stream discharge from permafrost thawing in the Yukon River basin: Potential impacts on lateral export of carbon and nitrogen. *Geophysical Research Letters*, *34*, L12402. http://dx.doi.org/10.1029/2007GL030216.

Whitcomb, J., Moghaddam, M., McDonald, K., Kellndorfer, J., & Podest, E. (2009). Mapping wetlands of Alaska from L-band SAR imagery. *Canadian Journal of Remote Sensing*, *35*(1), 54–72.

Willmott, C. J., & Matsuura, K. (2005). Advantages of the mean absolute error (MAE) over the root mean square error (RMSE) in assessing average model performance. *Climate Research*, *30*, 79–82.

Wylie, B. K., Pastick, N. J., Johnson, K. D., Bliss, N., & Genet, H. (2015). Chapter 3. Soil carbon and permafrost estimates and susceptibility in Alaska. In Z. Zhu, & A. D. McGuire (Eds.), *Baseline and projected carbon storage and greenhouse-gas fluxes in ecosystems of Alaska. USGS professional paper* (in press).

Yoshikawa, K., Bolton, W. R., Romanovsky, V. E., Fukuda, M., & Hinzman, L. D. (2003). Impacts of wildfire on the permafrost in the boreal forests of Interior Alaska. *Journal of Geophysical Research*, *108*, 8148.

Yoshikawa, K., & Hinzman, L. (2003). Shrinking therrnokarst ponds and groundwater dynamics in discontinuous permafrost. *Permafrost and Periglacial Processes*, *14*(2), 151–160.

Zhang, Y. (2013). Spatio-temporal features of permafrost thaw projected from long-term high-resolution modeling for a region in the Hudson Bay Lowlands in Canada. *Journal of Geophysical Research — Earth Surface*, *118*, 542–552. http://dx.doi.org/10.1002/jgrf.20045.

Zhang, Y., Chen, W., & Cihlar, J. (2003). A process-based model for quantifying the impact of climate change on permafrost thermal regimes. *Journal of Geophysical Research*, *108*, 4695. http://dx.doi.org/10.1029/2002JD003354.

Zhang, Y., Chen, W., & Riseborough, D. W. (2008). Disequilibrium response of permafrost thaw to climate warming in Canada over 1850–2100. *Geophysical Research Letters*, *35*(L02502), 15. http://dx.doi.org/10.1029/2007GL032117.

Zhang, Y., Olthof, I., Fraser, R., & Wolfe, S. A. (2014). A new approach to mapping permafrost and change incorporating uncertainties in ground conditions and climate projections. *The Cryosphere*, *8*, 1895–1935.

Zhang, Y., Li, J., Wang, X., Chen, W., Sladen, W., Dyke, L., et al. (2012). Modelling and mapping permafrost at high spatial resolution in Wapusk National Park, Hudson Bay Lowlands. *Canadian Journal of Earth Sciences*, *49*, 925–937. http://dx.doi.org/10.1139/E2012-031.